ACS NANO

www.acsnano.org

ARTICLE

Selective Enrichment of Full Capsids of Adeno-Associated Virus

Vivekananda Bal, Jacqueline M. Wolfrum, Paul W. Barone, Stacy L. Springs, Anthony J. Sinskey, Robert M. Kotin, and Richard D. Braatz*

Cite This: *ACS Nano* 2025, 19, 35348–35369

Read Online

ACCESS | Metrics & More | Article Recommendations | Supporting Information

ABSTRACT: Gene therapies using recombinant adeno-associated virus (rAAV) have been developed to treat monogenic and acquired diseases, but are currently the most expensive drugs, limiting patient access to these treatments. The drug pricing is due, in part, to high manufacturing costs. In addition to the discontinuous production process, the cells producing rAAV generate substantial quantities of empty (50−90%) and partially filled (indeterminant) capsids. These impurities do not contribute to the potency and increase the immunogenicity; therefore, empty particles must be removed prior to formulating the bulk drug substance. The conventional separation processes inefficiently separate the empty and partially filled capsids from the biologically active full capsids. These separation processes result in substantial product losses, scale poorly, and are expensive, time-consuming, and require additional processing steps. This Article describes a one-step separation method using selective crystallization—a process which, to our knowledge, has not been used previously for rAAV purification. The process does not physically/chemically modify the target component (full capsid), is highly efficient, highly scalable, and economical, and improves product quality. Hanging-drop vapor diffusion experiments are used to scout crystallization conditions in which full and empty capsids crystallize and then to define conditions in which crystals of full, empty, or both full and empty capsids nucleate and grow. The experimental results for rAAV serotypes 5, 8, and 9 as exemplary vectors and scale-up results show that full capsids can be selectively crystallized and separated from a mixture of full, partially filled, and empty capsids as well as other protein and salt impurities with full capsid enrichment of >80%, approximately 20% higher than the existing methods, and a yield of >90%, while maintaining biological activity. The selective crystallization process rapidly (<4 h) achieves greater enrichment of full capsids in a single step than previously reported protocols. Importantly, incorporating the selective crystallization process into cGMP vector production would accelerate production timelines and substantially reduce costs by eliminating the need of specialized immunoaffinity chromatography media.

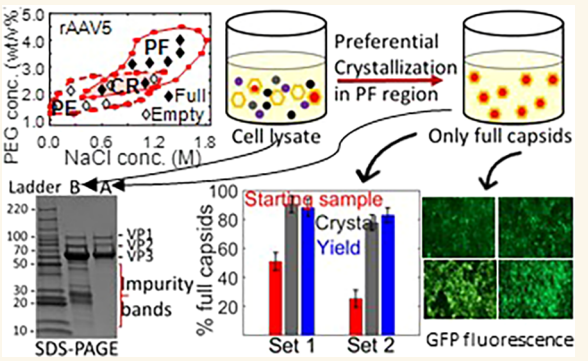

KEYWORDS: *protein purification, protein crystallization, gene therapy, adeno-associated virus, selective crystallization, biomaterial characterization, bioassays*

INTRODUCTION

Recombinant adeno-associated virus vectors (rAAVs) have demonstrated clinical benefits for patients affected by retinopathies (Leber's congenital amaurosis), coagulopathies (hemophilia), and neurological diseases (aromatic amino acid deficiency and spinal muscular atrophy).[1] Greater than 70% of the gene therapies currently approved by drug regulatory agencies globally are viral-vector-based.[2−4] The largest class of these gene therapies are based on rAAVs, which are the focus of >200 clinical trials.[3]

Depending on the transgene, capsid composition, and manufacturing platform, the recovered rAAV particles may initially contain 50% to 90% empty capsids (particles that do not contain the therapeutic transgene) (Figure 1a) along with an indeterminant percentage of partially filled capsids.[5−7] The empty capsids provide no therapeutic benefit, increase the capsid antigen load, reduce the transduction efficiency, and contribute to immune responses such as thrombotic microangiopathies (TMAs).[8−10] These observations have stimulated the development of methods for removing empty capsids to

Received: January 9, 2025
Revised: August 31, 2025
Accepted: September 4, 2025
Published: September 29, 2025

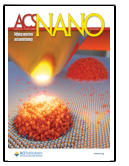

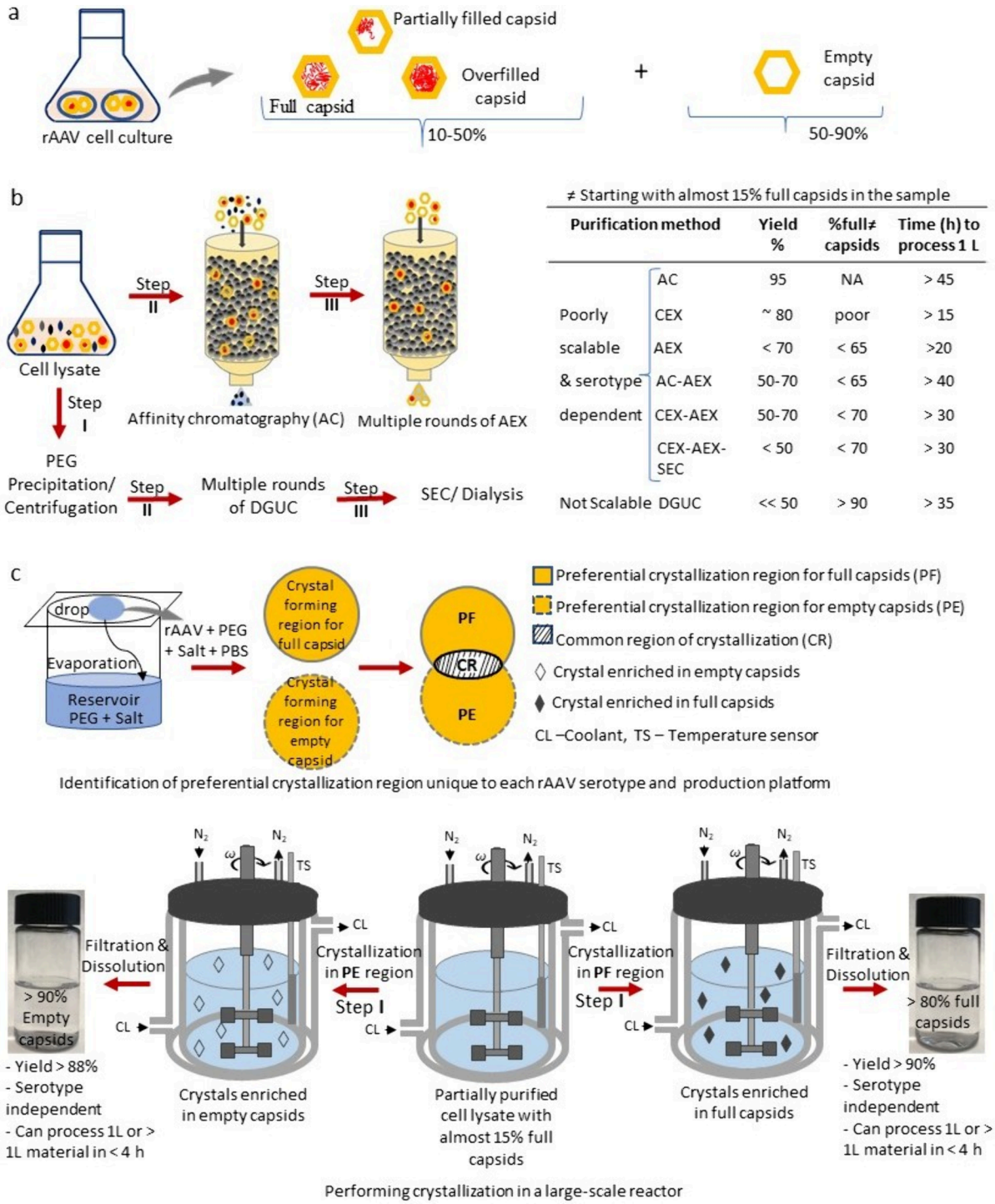

Figure 1. Schematic of purification/separation of either full or empty capsids from their mixture/partially purified cell lysate. (a) Production of rAAV capsids in cells suspension. (b) Schematic of industrial-scale separation/purification of full capsids with table showing the percentage yield/recovery, enrichment achieved (% full capsids), and time required to process 1 L of cell lysate material. (c) Proposed idea of selective crystallization-based purification: identification of preferential crystallization region for full capsids and for empty capsids and performing preferential crystallization experiment to separate full capsids and empty capsids from a partially purified cell lysate. Captions showing the enrichment (% full capsids or % empty capsids) and yield/recovery achieved after preferential crystallization and the corresponding processing time for 1 L or >1 L partially purified cell lysate. Key: AC—affinity chromatography, CEX—cation exchange chromatography, AEX—anion exchange chromatography, SEC—size exclusion chromatography, DGUC—density gradient ultracentrifugation, rAAV—recombinant adeno-associated virus, PEG—polyethylene glycol, PBS—phosphate buffer saline, PF—preferential crystallization region for full capsids, PE—preferential crystallization region for empty capsids, CR—common region of crystallization, TS—temperature controller, CL—coolant, N_2—nitrogen gas, ω—rpm.

improve the efficacy and safety of the therapy. However, separating empty and particularly partially filled capsids from full capsids is extremely challenging, due to the very similar physical properties, such as size, density (1.41 g/cm^3 for full

https://doi.org/10.1021/acsnano.5c00566
ACS Nano 2025, 19, 35348−35369

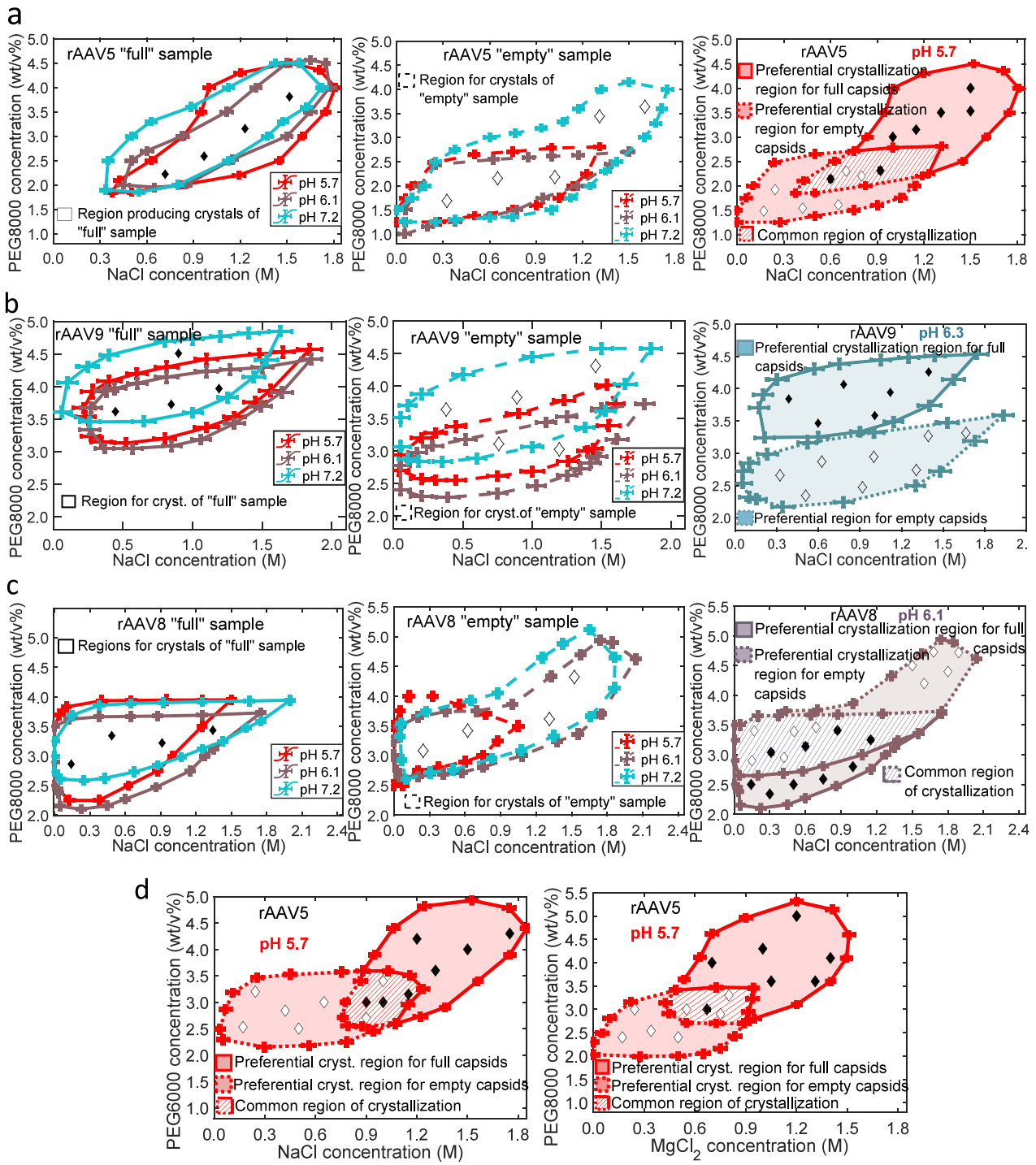

Figure 2. Identification of preferential crystallization region for full and empty capsids of Sf9-produced rAAV. (a) Phase diagram for full capsids (left) and empty capsids (middle) of rAAV5 at different pH and the corresponding preferential crystallization region (right) at pH 5.7. (b) Phase diagram for full capsids (left) and empty capsids (middle) of rAAV9 as a function of pH and the corresponding preferential crystallization region (right) at pH 6.3. (c) Phase diagram for full capsids (left) and empty capsids (middle) of rAAV8 at different pH and the corresponding preferential crystallization region at pH 6.1. (d) Effect of PEG6000 (left) and $MgCl_2$ (right) on the preferential crystallization regime of rAAV5 capsids at pH 5.7. In all cases, length of the transgene was 2.46 kbp. □ represents the enclosed crystallization region, ◆ represents the full capsid crystals, and ◊ represents the empty capsid crystals. All the experimental data points include the error bars, which represent the mean and standard deviations (as represented by x_{error} and y_{error}) from the three experimental replicates. The range of x_{error} and y_{error} are (±0.025 − ±0.036) and (±0.051 − ±0.073) for the rAAV5 "full" sample, (±0.027 − ±0.038) and (±0.055 − ±0.073) for the rAAV5 "empty" sample, (±0.063 − ±0.086) and (±0.062 − ±0.084) for the rAAV9 "full" sample, (±0.050 − ±0.081) and (±0.051− ±0.075) for the rAAV9 "empty" sample, (±0.021 − 0.039) and (±0.055 − ±0.074) for the rAAV8 "full" sample, (±0.028 − ±0.039) and (±0.053 − ±0.075) for the rAAV8 "empty" sample, (±0.021 − ±0.034) and (±0.056 − ±0.072) for the rAAV5 PEG600 effect, and (±0.020 − ±0.035) and (±0.054 − ±0.070) for the rAAV5$MgCl_2$ effect.

https://doi.org/10.1021/acsnano.5c00566
ACS Nano 2025, 19, 35348−35369

and 1.31 g/cm^3 for empty, assuming 4.7 kbp virion genome), and isoelectric point (5.9 for full and 6.3 for empty).[11,12] Chromatography and ultracentrifugation are widely used to purify/enrich full particles (Figure 1b).[13,14] Ultracentrifugation (UC) exploits the difference in buoyant density, and ion-exchange chromatography (IEX) exploits the difference in isoelectric point between full and empty capsids. But these conventional methods do not effectively remove empty and partially filled capsids. Additionally, they are poorly scalable and incur high costs and involve long processing times, additional manipulations, and higher product losses, which make them unsuitable for use in commercial clinical-grade vector production.[15−17]

Here we propose that the slight differences in charge density, contributed by the nucleic acids in vector genomes, (Supplementary Figures 1 and 2) are sufficient for preferential crystallization of full rAAV capsids. The process provides a scalable and economical method for rAAV capsid purification compatible with the commercial industrial-scale used in conventional purification methods. In addition, the use of high purity reagents, e.g., NaCl and PEG (polyethylene glycol), would integrate into a clinical grade vector production, i.e., cGMP compliant processes. Though preferential crystallization is common in the small molecule pharmaceutical industry, it has not been previously described for biologics purification, and this is the first time preferential crystallization has been performed without physically/chemically modifying the target component (i.e., full capsids in this case). The salt, pH, and organic precipitant provide "levers" that may be manipulated to influence the charge density surrounding each capsid and the charged interactions between full, partially filled, and empty capsids. The solution pH has a strong effect on capsid surface charge density, whereas salt influences the charge environment around the capsid by controlling the electrical double-layer thickness/zeta-potential, just as for other proteins (Supplementary Figures 1 and 2).[18−22] As such, salt concentration controls the rate of crystallization by shielding capsid's inherent charge density, just as for protein molecules.[23−29] Together, pH and salt concentration thus directly control the capsid-to-capsid interactions and hence the solubility and crystallization rates of full, partially filled, and empty capsids.

In this article, we identify solution conditions for the preferential crystallization of full and empty capsids of AAV serotypes 5, 8, and 9 as exemplary vectors. To establish a higher resolution "picture" of crystallization conditions, a wide range of precipitant and pH concentrations were screened in a hanging-drop vapor diffusion system (Supplementary Figures 3 and 4), and a phase diagram is constructed for both "full" and "empty" capsid samples (Figure 1c and Supplementary Figure 4). To identify the preferential crystallization conditions, phase diagrams for both "full" and "empty" capsids were plotted in the same figure. This clearly shows the overlapped region (common region), where both full and empty capsids cocrystallize, and the preferential crystallization regions for full capsids and for empty capsids (Figure 1c). Once the preferential crystallization region for full capsids is identified, crystallization experiments were performed under those conditions to separate full capsids, which were subsequently redissolved for further characterization. The preferential crystallization regions are specific to each serotype and the production platform (i.e., *Spodoptera frugiperda* (Sf9) or human embryonic kidney (HEK293) cells); however, once established, they can be used to preferentially crystallize full capsids from the partially purified cell lysate without the need of rederiving the preferential crystallization conditions. Crystallization is highly sensitive to the solution conditions as well as the capsid surface features such as the surface structure and chemistry, protein amino acid sequence, surface post-translational modifications (PTMs), and charge density. Changes in the level of PTMs in capsids lead to the change in the charge density (solubility) and the number of degrees of freedom/conformations, which influence the nucleation/crystallization propensity or crystallizability. As per literature reports, production platforms and the downstream processing conditions affect the types and extent of the PTM level of the capsids produced and hence crystallizability/crystallization propensity.[30,31]

RESULTS AND DISCUSSION

Construction of Phase Diagram and Preferential Crystallization Region. PEG and NaCl are the most commonly used precipitants for protein crystallization.[32−34] The NaCl influences the protein solubility by the "salting in" and "salting out" effects, whereas the PEG functions as an aquacide effectively concentrating the proteins by reducing the solvent volume.[35]

Figure 2a-c (column 1 and 2) shows the corresponding phase diagrams for "full" and "empty" capsids of rAAV5, rAAV9, and rAAV8, respectively, as a function of pH, PEG8000, and NaCl concentrations (see supplementary Figures 5−8 for phase diagrams at pH 5.7, 5.9, 6.1, 6.3, and 7.2). The graphical representation reveals that crystallization occurs within a closed and bounded region. Empty and full capsids of different serotypes show appreciably different solution behavior depending on pH and NaCl and PEG8000 concentrations. Higher charge density on the full capsids compared to the empty capsids for rAAV serotypes 5 and 9 tends to increase the solubility, and this causes the crystallization of full capsids to occur at relatively higher PEG and NaCl concentrations. In contrast, significant post-translational modifications (PTMs) of the empty capsids compared to full capsids for rAAV8 (Supplementary Figure 9) tend to increase solubility for empty capsids (as observed in other molecules or compounds[36−38]) requiring higher PEG and NaCl concentrations to crystallize empty AAV8 capsids (Figure 2c).

Regions, where either full or empty rAAV particles can be preferentially crystallized and the common regions, where both empty and filled capsids cocrystallize, are clearly observed in Figure 2a-c column 3 for best-case conditions and in Supplementary Figure 10 for each pH value tested. The pH values in these experiments were chosen to be near the isoelectric point of full and empty rAAV, i.e., where the net charge on the surface is zero (i.e., zero zeta-potential, Supplementary Figure 2) and the capsids have the lowest solubility just as for other proteins.[39−42] These preferential regions depend on pH and PEG and NaCl concentrations and the net charge of the assembled coat proteins and the DNA within the capsid.

Additionally, other precipitants were evaluated for differential crystallization of rAAV capsids. Crystallization conditions were screened using PEG6000 and NaCl as well as PEG8000 and $MgCl_2$ (Figure 2d) as precipitants to test whether the molecular weight of PEG or the valence/ionic strength affects the preferential crystallization process. Thus,

https://doi.org/10.1021/acsnano.5c00566
ACS Nano 2025, 19, 35348−35369

PEG6000 and $MgCl_2$ were chosen arbitrarily. Both cases show that full and empty capsids can be preferentially crystallized from a mixture. As such, the preferential crystallization was not sensitive to the molecular weight of PEG or the valency of inorganic salt.

Confirmation of Crystallinity of Particles. A solubility analysis shows that the visible particles are composed of capsids rather than NaCl or PEG (Supplementary Figure 11). To determine whether coformulation of NaCl and PEG affects the solubility of either component,[43−46] a set of control experiments was performed for the combinations across the full ranges of PEG concentration (0.5 to 8 wt/v%) and NaCl concentration (0.005 to 2.5 M) in the absence of rAAV capsids. No crystals were observed under these conditions, confirming that rAAV capsids were essential for crystallization. A study of crystal birefringence in cross-polarized light microscopy (Supplementary Figures 12 and 13) shows that the particles are crystalline.

Quantitative Evaluation of Enrichment of Full and Empty Capsids after Preferential Crystallization. To evaluate quantitatively the enrichment of full or empty capsids after preferential crystallization, ddPCR and ELISA experiments were performed on dissolved crystals, and the fractions (expressed as percentages) of full and empty capsids were calculated for different experimental conditions at each pH as shown in Supplementary Figures 14−17 for starting sample with different fractions of full and empty capsids. In Supplementary Figures 14−17, the percentage of enrichment associated with each experimental condition represents the mean from three experimental replicates with 2−3% standard deviation. Tables 1 and 2 show the mean and standard deviation of percentages shown in Supplementary Figures 14−17 for each starting concentration of full capsids and empty capsids. Conditions resulting in preferential crystallization of full capsids results in a higher fraction of full capsids in crystals regardless of the fraction of full capsids in the starting sample. Significantly, 74−80% full capsid enrichment can be achieved starting with 20% full capsids (Table 1) by preferential crystallization. Obtaining greater enrichment is possible if the starting fraction of full capsids is higher. For example, a starting sample with about 80% full capsids can be increased to >94% full capsids in the crystals. Likewise, preferential crystallization of empty capsids (Table 2) results in crystals enriched with 71−78% empty capsids starting with ∼20% empty capsids. Similar analysis was performed for rAAV9 and rAAV8 crystals. Here too, preferential crystallization produces crystals enriched to ∼ 0−75% full capsids starting with about 19% full capsids. Thus, conditions were established represented by the preferential regions that can be applied to selectively crystallize either empty or full capsids from the mixed populations of empty and full capsids.

Table 1. Enrichment of Full Capsids in Crystals Obtained by Preferential Crystallization of Full Capsids of Sf9-Produced rAAV with Different Fractions of Full Capsids in the Starting Sample[a]

Serotypes	79 ± 3.5% full capsids in starting sample	50 ± 2.5% full capsids in starting sample	15.1 ± 2.8% full capsids in starting sample
rAAV5	97 ± 3	90 ± 4.5	81 ± 2.5
rAAV9	98 ± 2.5	89 ± 4	82 ± 3.4
rAAV8	–	–	82 ± 2.1

[a]**Note:** Mean and standard deviation of the percentages of full capsids in the crystals obtained after crystallization in different crystallization conditions (>9; as shown in Supplementary Figures 14, 16, and 17) in the preferential crystallization region of full capsids of Sf9-produced rAAV for starting samples with different fractions of full capsids. % of full capsid corresponding to each experimental condition in Supplementary Figures 14, 16, and 17 represents the mean from three experimental replicates.

Table 2. Enrichment of Empty Capsids in Crystals Obtained by Preferential Crystallization of Full Capsids of Sf9-Produced rAAV with Different Fractions of Full Capsids in the Starting Sample[a]

Serotypes	79 ± 3.5% empty capsids in stating sample	50 ± 2.5% empty capsids in stating sample	15 ± 2.4% empty capsids in stating sample
rAAV5	97.5 ± 5	90 ± 4	78 ± 2.5
rAAV9	96.5 ± 4	89 ± 3	79.5 ± 4
rAAV8	–	–	81.9 ± 1.5

[a]**Note:** Mean and standard deviation of percentages of empty capsids in the crystals obtained after crystallization in different crystallization conditions (>9; as shown in Supplementary Figures 15 and 17) in the preferential crystallization region of empty capsids of Sf9-produced rAAV for starting sample with different fraction of empty capsids. % of empty capsid corresponding to each experimental condition in Supplementary Figures 15 and 17 represents the mean from three experimental replicates.

To investigate the morphology of capsid after crystallization, TEM images of the crystallization-purified sample were obtained (Supplementary Figures 18hjl). The micrographic images indicate that capsids are homogeneous in shape and size with a diameter of ∼22−25 nm. Comparison of the TEM image of the crystallization-purified sample with that of the reference sample (Supplementary Figures 18a-d) shows that capsids morphology remains unaffected by the crystallization process. Although not designed as a quantitative assay, the percentage of full and empty capsids after preferential crystallization was calculated based on a total of ∼2500 capsid particles from multiple TEM fields. This analysis suggests that the full capsid's preferential crystallization-purified sample contains >85% full capsids (Supplementary Figures 18fj) as compared to 20−25% full capsids in the starting sample (Supplementary Figures 18ei). Likewise, the empty capsid's preferential crystallization results in >90% empty capsids (Supplementary Figures 18hl) from a starting sample of 20−25% empty capsids (Supplementary Figures 18gk). Thus, TEM image analysis also supports the full-empty percentage obtained using ddPCR and ELISA analyses.

The enrichment of full and overfilled capsids after crystallization within the preferential crystallization region of full capsids is further supported by mass photometry results (Supplementary Figures 19−21), which shows that a starting sample of rAAV9 of ∼74% full + overfilled is enriched to about 97% full + overfilled (Supplementary Figure 19); a starting sample of rAAV5 of ∼39% full + overfilled capsids is enriched to about 84% full + overfilled (Supplementary Figure 20). Three analytical replicates of the mass photometry experiment in SamuxMP (Refeyn Ltd., MA, USA) suggests that the variation in measurement is <1.5%.

Effect of Production Platform on the Preferential Crystallization Region and Selectivity. As reported in the literature,[30,31,47] rAAV capsids may undergo PTM, e.g., glycosylation, phosphorylation, etc. The extent of PTMs may

https://doi.org/10.1021/acsnano.5c00566
ACS Nano 2025, 19, 35348−35369

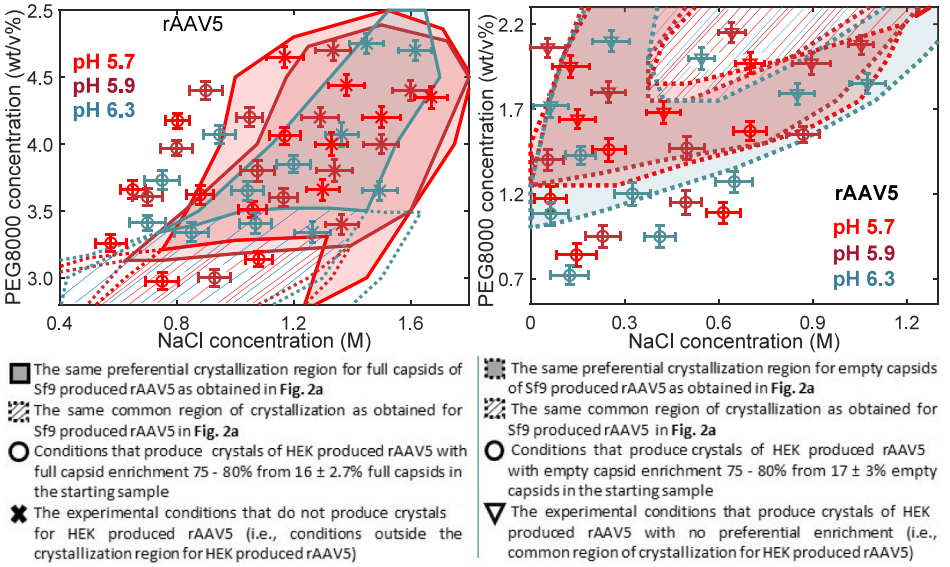

Figure 3. Comparison of preferential crystallization conditions/regions between rAAV capsids produced in Sf9 and HEK293 cells. Left figure: Comparison of preferential crystallization region of full capsids of HEK293-produced rAAV5 (as shown by the successful experimental data points as represented by circles with error bars) with that of the full capsids of Sf9-produced rAAV5 (as shown by the solid filled area). Right figure: Comparison of preferential crystallization region of empty capsids of HEK293-produced rAAV5 (as shown by the successful experimental data points as represented by the circles with error bars) with that of the empty capsids of Sf9-produced rAAV5 (as shown by the solid filled area). All the error bars represent the mean and standard deviation from three experimental replicates. Three analytical replicates for ddPCR suggest that the variation in measurement is insignificant (<1%). See rAAV Samples section in the Methods and Experiments section for the detailed description of the samples.

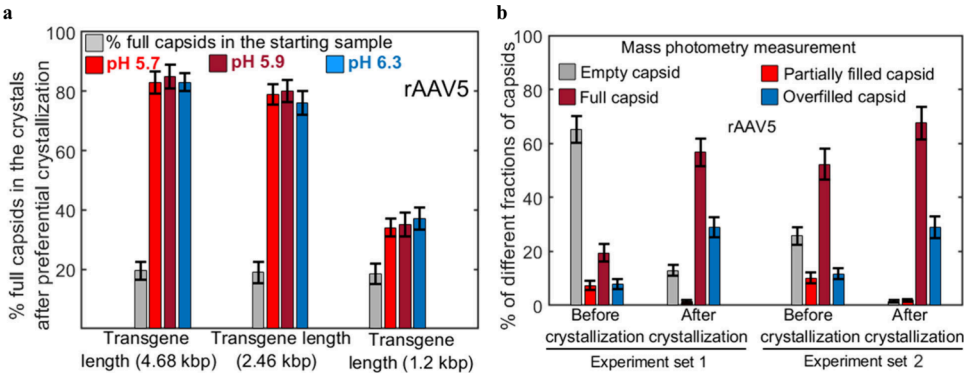

Figure 4. (a) Enrichment of full capsids obtained after crystallization in the preferential crystallization region of Sf9-produced rAAV5 full capsids for three systems: full capsids carrying transgene 4.68 kbp, 2.46 kbp, and 1.2 kbp. Bar plots showing the mean and standard deviation of percentages of full capsids in crystals obtained after crystallization in different crystallization conditions in the preferential crystallization region as shown in Supplementary Figure 25. Three analytical replicates of ddPCR measurement (CBI, MIT) suggest that the variation in measurement is insignificant (<1%). (b) Percentage of empty, partially filled (1.2 kbp), full (2.46 kbp), and overfilled (4.68 kbp) rAAV5 capsids in the mixture before and after crystallization in the preferential crystallization region of full capsids as measured in mass photometry (Supplementary Figures 26−27). Bar plots showing the mean and standard deviation from three experimental replicates. Three analytical replicates of mass photometry measurement in SamuxMP (Refeyn, MA) suggest that the variation in measurement is insignificant (<1.5%). Experimental conditions: 3.5% PEG8000, 1.3 M NaCl at pH 5.7 (Experiment set 1) and 3% PEG8000, 1.2 M NaCl at pH 6.1 (Experiment set 2). See rAAV Samples section in the Methods and Experiments section for detailed description on the production platform and purification methods used by the supplier.

be influenced by processing, e.g., time of harvest, or production platform, e.g., HEK293 or Sf9 cells, or the postproduction purification methods.[48] Being extremely sensitive to surface-exposed substances and surface features and charge density,[36] crystallization conditions may be influenced by the presence and extent of capsid PTMs. An experiment was performed with HEK293-produced rAAV5 capsids as an example and compared with the preferential crystallization region as obtained for Sf9-produced rAAV5 in Figure 2a (Supplementary Figure 5) to evaluate whether the conditions for preferential crystallization depends on the production methods. The corresponding experimental results shown in Figure 3 (see Supplementary Figures 22−23 for individual plots) suggest that, for HEK293-produced rAAV also, full or empty capsids can be preferentially crystallized out of a mixed population and the experimental conditions for preferential crystallization (as shown by the data points represented by the circular marker with error bars) are slightly different for Sf9 and HEK293 cell-produced rAAV5 (as shown by the regions enclosed by solid lines for full capsids and dotted lines for

https://doi.org/10.1021/acsnano.5c00566
ACS Nano 2025, 19, 35348−35369

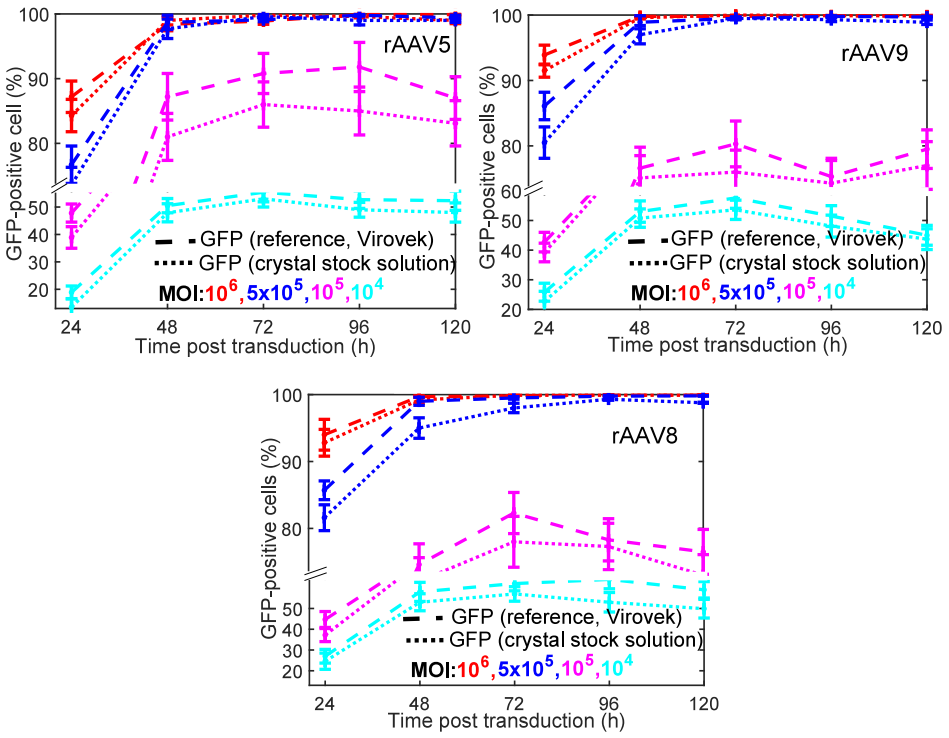

Figure 5. Flow cytometry experiment results showing the variation of percentage of GFP-positive cells as a function of post transduction time for the transduction of HEK293 cell suspension with crystal stock solution as prepared from the crystals obtained after preferential crystallization of full capsids of Sf9-produced rAAV5, rAAV9, and rAAV8 and transduction with the reference rAAV sample (Virovek). In all cases, cell viability remains well above 90% throughout 5 days (Supplementary Figure 28). For all the serotypes evaluated, the full capsid transgene length was 2.46 kbp. Experimental conditions for preferential crystallization of full capsids: 4% PEG8000, 1.2 M NaCl at pH 5.7 for rAAV5 for a starting sample with 33% full capsids; 4% PEG8000, 0.6 M NaCl at pH 6.3 for rAAV9 for a starting sample with 37% full capsids; and 2.5% PEG8000, 0.6 M NaCl at pH 6.1 for rAAV8 for a starting sample with 41% full capsids. All the error bars represent the mean and standard deviation from three experimental replicates. Three analytical replicates of the flow cytometry measurement in Aria 4 (Flow core, Koch Institute, MIT) indicate that the variation in the measurement is insignificant (<2%).

empty capsids). The conditions for preferential crystallization were not always transferable between AAV5 vectors produced in Sf9 and HEK293 cells (Figure 3). These unsuccessful preferential crystallization conditions are shown by the data points represented by the cross markers with error bars and downward-pointing triangle marker with error bars. LC-MS (liquid chromatography−mass spectrometry) was performed to compare the extent of PTMs in Sf9 and HEK293-produced rAAV capsids (Supplementary Figure 24).

The data indicate that rAAV5 capsid PTMs are similar but with slight differences appearing between the Sf9 and HEK293-produced vectors (Supplementary Figure 24). Since the postprocessing conditions remain the same, the difference in the extent of the PTMs is attributed to the production platform (see sample section in methods section). However, without evaluating multiple vector batches from the same and different facilities, no conclusion can be drawn about capsid PTMs produced in Sf9 or HEK293 cells. Results suggest that even a small difference in PTMs level is probably sufficient to cause a notable change in preferential crystallization conditions as the crystallization process is highly sensitive to the capsid structure, conformations and solubility, which are influenced by the external PTMS level.[36−38,49,50] The ddPCR and ELISA analyses suggest that the enrichment of full capsids for HEK293-produced rAAV can be 75−80% for a starting sample with around 19% full capsids. Thus, the preferential crystallization method itself and the capsid enrichment are not influenced by the vector source or quality of rAAV or PTMS level.

Effect of Transgene Length on the Preferential Crystallization and Selective Removal of Partially Filled Capsids. The virion genome contributes to the vectors mass and net charge; therefore, to understand the effect of transgene length on preferential crystallization and the corresponding enrichment, an experiment was performed with rAAV5 capsids carrying transgene of length half (1.2 kbp) and twice (4.68 kbp) the size of the full-length, wild-type virion genome (2.46 kbp). Results (Figure 4a) suggest that the enrichment of capsids with transgene 1.2 kbp is almost half of the enrichments of capsids with transgene 2.46 kbp and the enrichment/selectivity becomes independent of transgene length above a certain transgene size. This suggests that the preferential crystallization kinetics/selectivity is strongly dependent on transgene length. Thus, by maintaining the conditions in the preferential crystallization region of full capsids, full capsids can be selectively separated from the empty and partially filled capsids, whose therapeutic efficiency is questionable.[51−53] The literature on commercial purification methods such as IEX and UC do not explicitly talk about the removal of partially filled capsids, probably because of the process inefficiency and difficulty associated with measurement.[13,14,54] High selectivity of full capsids is most probably due to the strong dipolar nature of overall charge because of the noncentric alignment of the DNA inside a capsid as observed in other DNA viruses.[55] This allows the faster

https://doi.org/10.1021/acsnano.5c00566
ACS Nano 2025, 19, 35348−35369

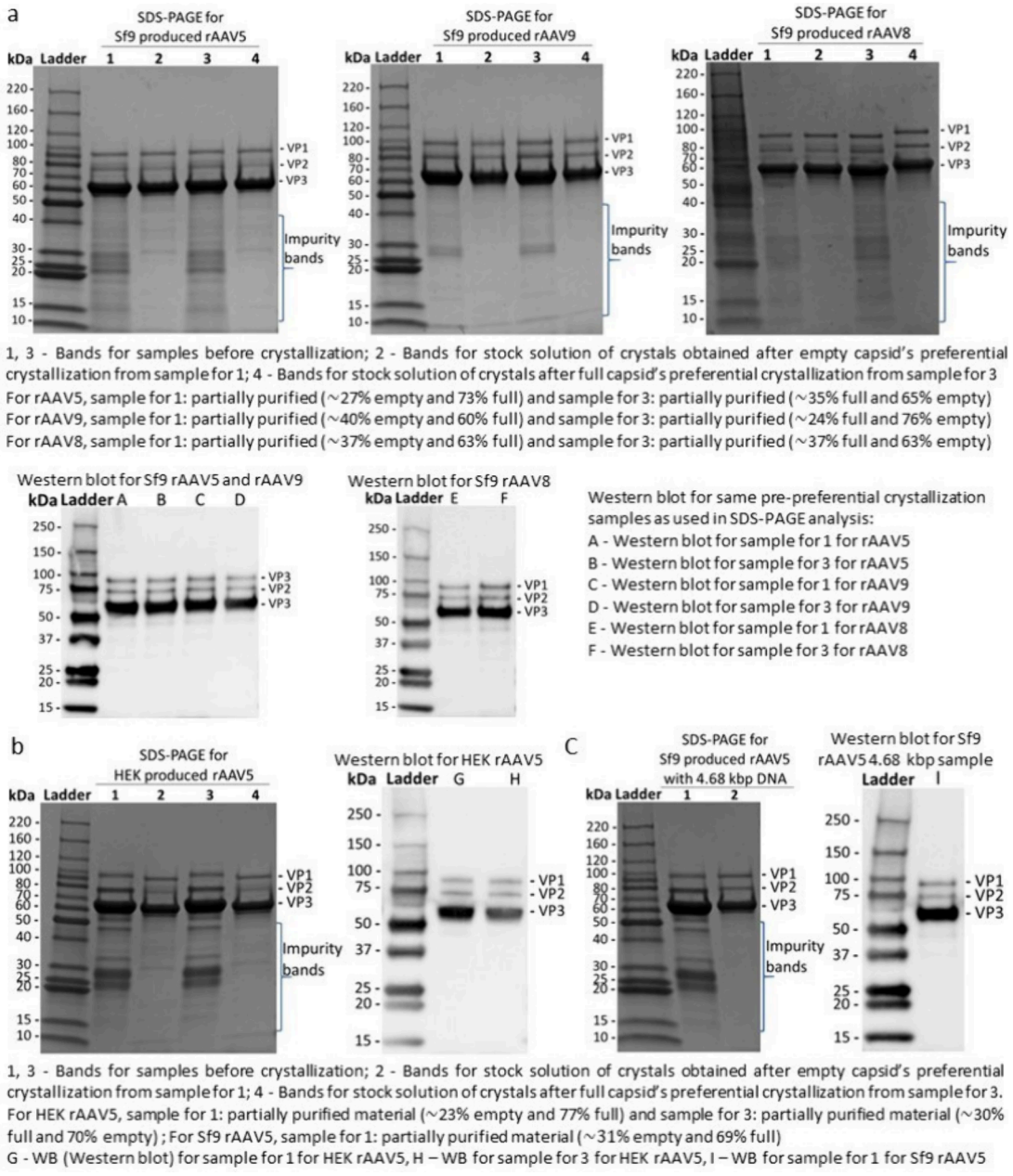

Figure 6. Capsid protein composition assessment using SDS-polyacrylamide electrophoresis. (a) row 1: SDS-PAGE gel electrophoresis with Coomassie blue stain results before and after preferential crystallization of full and empty capsids of sf9-produced rAAV5 (left image), rAAV9 (middle image), and rAAV8 (right image) showing the capsid protein components, VP1, VP2, and VP3, and protein impurities. row 2: The corresponding Western blot results for samples before preferential crystallization identifying only the viral protein components, VP1, VP2, and VP3 and confirming that the other protein bands as observed in SDS-PAGE electrophoresis as protein impurities from cell lysis. (b) SDS-PAGE gel electrophoresis with Coomassie blue stain before and after preferential crystallization of full and empty capsids of HEK293-produced rAAV5 (left) and the corresponding Western blot results for the samples before preferential crystallization (right). (c) SDS-PAGE electrophoresis with Coomassie blue stain before and after preferential crystallization of full capsids (4.68 kbp) of Sf9 rAAV5 (left) and the corresponding Western blot results (right). SDS-PAGE and Western blot experiments were repeated at least three times and the highest resolution results are presented in the figure. (See Supporting Information for experimental conditions, see Supplementary Figures 33−34 for SDS-PAGE with silver staining results and see the rAAV Samples section in the Methods and Experiments section for detailed description on the production platform and purification methods used for the samples by the Supplier).

alignment/arrangement of full capsids in an orderly manner to form crystals resulting in higher crystallization propensity and higher selectivity. For partially filled capsids, the weak dipolar nature reduces the propensity of crystallization and results in hence poor selectivity.

To further validate the preferential removal of the partially filled capsids along with the empty capsids, a set of crystallization experiments were performed in the preferential crystallization conditions of full capsids of rAAV5 for a starting sample containing empty, partially filled (1.2 kbp), full (2.46 kbp), and overfilled (4.68 kbp) capsids. Mass photometry was used to measure the percentage of different fractions of capsids before and after the preferential crystallization. The corresponding experimental result is shown in Figure 4b (see

https://doi.org/10.1021/acsnano.5c00566
ACS Nano 2025, 19, 35348−35369

Supplementary Figures 26−27 for mass photometry data). It shows that the percentages of both empty and partially filled capsids in the mixture are significantly reduced after preferential crystallization, while the percentages of full and overfilled capsids show a significant rise. This supports the conclusion in Figure 4a and suggests that the preferential crystallization selectively removes empty and partially filled capsids.

Effect of Preferential Crystallization on Biological Activity of Capsids. To understand the effect of crystallization on biological activity, full rAAV5, rAAV8, and rAAV9 crystals were dissolved and used to transduce HEK293 cell suspension and analyzed for reporter gene, GFP, expression (Figure 5) and viability (Supplementary Figure 28) based on singlet cell population using flow cytometry every 24 h for 5 days. For each serotype, viability and transduction efficiency (% GFP-positive cells) are comparable to that of the positive control (from Virovek) for all MOIs throughout the 5 days. In all cases, cell viability remains above 90% throughout the experiment ensuring that all the statistics are based on high population of live cells. It is observed that, for an MOI of 10^6, >85% of viable cells are transduced within 24 h, while only ∼15% of viable cells are transduced in the same period of time when the virus dosage is reduced by an order of 2 (i.e., MOI 10^4), and the transduction rate is so slow that only 40−50% of viable cells are transduced at day 5. These results demonstrate that biological activity of capsids remains preserved after crystallization and dissolution. Further HEK293T cells were transduced with dissolved crystal; cells were observed under fluorescence microscope every 24 h for 5 days, and transduction efficiency was measured on day 5 (Supplementary Figures 29, 30, and 31). In nearly all cases, weak GFP fluorescence intensity appeared after 24 h, reaching maximum fluorescence intensity at day 4 with MOIs of 10^5 and 10^6 approaching the transduction limit. For all serotypes, transduction efficiency agrees well with that of the positive control (from Virovek), indicating that biological activity and stability of the full capsids are preserved during crystallization and after dissolution.

Transduction experiments, analogous to tissue culture infectious dose (TCID50) assays, were performed to obtain a more precise value of the biologically active vector titer. The biologically active vector titer for crystal stock solution is found to be close to that of the positive control (Supplementary Figure 32 & Supplementary Table 1), demonstrating that the biological activity of full capsids remains preserved even after crystallization.

Analysis of Purity of Crystals and Integrity of Capsid Proteins. SDS-PAGE gel electrophoresis was performed to assess vector purity and determine integrity of capsid proteins (Figure 6) following crystallization. These images confirm the presence of all three VP proteins VP1, VP2, and VP3 in the crystallized capsids, and the quantification of proteins indicates that the ratio of the VPs in the crystallized sample remains essentially unchanged following crystallization for each serotype. The images also suggest that all the vector samples (see the rAAV Samples section in the Methods and Experiments section for detailed description of the samples) contain a significant amount of low-molecular-weight protein impurities (Figure 6 and Supplementary Figures 33 and 34), which are removed by the preferential crystallization. To confirm if the protein impurities appearing as Coomassie blue stained bands at molecular weight 20−30 kbp and 40 kbp are fragments of VP proteins, Western blot (Figures 6) was performed, and the results confirm that the impurities are not fragments of VP proteins. Thus, other protein impurities, which seem to originate during cell lysis and conventionally are removed by affinity chromatography, are also removed by preferential crystallization, eliminating the need of the former. This shows that the preferential crystallization directly from partially purified cell lysate leaves/rejects the impurities/cell lysis materials in the solution and selectively crystallizes/purifies the full capsids.

Point EDAX (energy dispersive X-ray analysis) was performed to establish the elemental composition of crystals at three different locations (Figure 7 and Supplementary Table 2), and the corresponding average of the elemental compositions in the three locations is shown in Table 3.

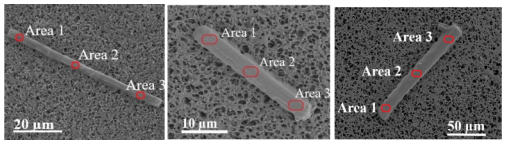

Figure 7. SEM images of rAAV5 (left), rAAV9 (middle), and rAAV8 (right) crystals at magnification showing the locations of EDAX analysis. Preferential crystallization conditions for full capsids: 3% PEG8000, 1.4 M NaCl, pH 5.7 for rAAV5 for a starting sample with 26% full capsids; 4% PEG8000, 1 M NaCl, pH 5.7 for rAA9 for a starting sample with 23% full capsids; 2.5% PEG8000, 0.3 M NaCl, and pH 6.1 for rAAV8 for a starting sample with 35% full capsids.

Table 3. Mean and Standard Deviation of Elemental Compositions (Supplementary Table 2) Obtained from EDAX Analysis at Three Different Locations on Crystals of Full Capsids as Shown in Fig. 7[a]

Elements	rAAV5 (atomic %)	rAAV9 (atomic %)	rAAV8 (atomic%)
C K	56.15 ± 0.340	55.30 ± 1.231	54.86 ± 0.520
N K	12.83 ± 0.598	12.92 ± 1.116	13.99 ± 0.376
O K	23.14 ± 0.189	23.92 ± 0.423	23.5 ± 0.632
Na K	0.93 ± 0.091	1.00 ± 0.136	0.82 ± 0.163
P K	3.17 ± 0.140	3.02 ± 0.228	3.00 ± 0.150
S K	2.92 ± 0.375	2.93 ± 0.262	3.00 ± 0.128
Cl K	0.87 ± 0.045	0.90 ± 0.104	0.83 ± 0.307
K K	0.02 ± 0.007	0.04 ± 0.003	0.06 ± 0.006

[a]**Note:** Elemental composition in each location on a crystal as provided in Supplementary Table 2 represents the mean from three analytical replicates of measurement in Octane Elect Super Detector (MIT nano, Material Science, MIT) with negligible standard deviation of 0.0005.

EDAX indicates that the major element in the crystal is carbon (atomic% ∼ 55) followed by oxygen (atomic% ∼ 23) and nitrogen (atomic% ∼ 13). This results in a ratio of ∼4.2:1.8:1 for C:O:N in capsid. These values are novel, and no elemental composition of capsid reports are in the literature. This is consistent as carbon and hydrogen are the two major constituent elements in any protein, followed by oxygen, nitrogen, and sulfur. Due to the low mass, EDAX does not detect hydrogen. The presence of a very small fraction of Na, K, and Cl (atomic% < 1) in crystals indicates that the crystal is high purity. Thus, preferential crystallization removes the salt

https://doi.org/10.1021/acsnano.5c00566
ACS Nano 2025, 19, 35348−35369

impurities too along with protein impurities, and empty and partially filled capsids.

Comparison of Time-Scales between Crystallization- and Chromatography-Based Purification Platforms. The crystallization process in hanging-drop may require 1 to 2 weeks for crystal to nucleate followed by 2−3 days for crystal growth, due to slow evaporation. In industrial crystallization, seed-crystals are used to induce/promote secondary nucleation, accelerating the time for crystal nucleation (see the Methods and Experiments section for a detailed description on crystal seeding, primary and secondary nucleation). Seeding experiments (Figure 8) were performed to determine the time

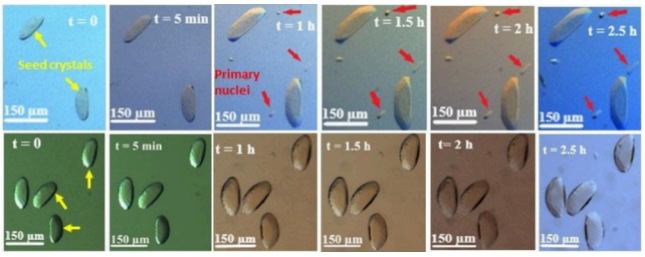

Figure 8. Growth of seed crystals and primary nuclei of full capsids of Sf9-produced rAAV5 (row 1) and rAAV9 (row 2) in the preferential crystallization region/condition. Experimental condition: 1.4 M NaCl, 4% PEG8000 at pH 5.7 for rAAV5 (row 1), and 1 M NaCl and 3.75% PEG8000 at pH 6.3 for rAAV9 (row 2). The seeding experiment is repeated more than three times and the best-case result is presented.

required for the seed crystals (yellow arrow)/new crystals (primary nuclei; red arrow) to grow to a separable/filterable size (minimum ∼ 10 μm).[56] Figure 8 shows that the crystals take almost 1 to 1.5 h to grow by 50 μm. Thus, seed crystals will reduce the overall crystallization time from 2−3 weeks to <2−3 h. This suggests that the full capsids can be selectively crystallized from the partially purified material in just 2−3 h irrespective of the volume or length scale of the crystallizer, whereas the conventional purification methods need much longer time to separate/purify full capsids and are dependent on the volume of the column/centrifuge tube and the cell lysate. For example, to process 1 L of cell lysate material, affinity chromatography needs >45 h, cation exchange chromatography (CEX) needs >15 h, anion exchange chromatography (AEX) needs >20 h, CEX-AEX needs >30 h, CEX-AEX-SEC (size-exclusion chromatography) needs >30 h, and UC-based purification needs >30 h for the columns of geometry mentioned in the reference.[54,57−60] Additionally, AEX, CEX-AEX and CEX-AEX-SEC typically are performed following capsid capture/purification processing involving PEG precipitation/dialyzed/affinity chromatography, which further increases its overall processing time and results in poor yield/recovery. Likewise, the UC tube capacity limits the volume. Either CsCl isopycnic or iodixanol step gradients are relatively inefficient and incur large product losses, introduce toxic heavy metals (cesium), expose the product to additional manual processing steps, risk equipment failure (e.g., centrifugation prematurely terminated or centrifuge tube collapse), and are not scalable. In contrary, preferential crystallization has no such limitations and needs only partially purified material for the feed stream as the crystallization process itself removes impurities. These processing attributes represents an attractive alternative to multimodal processing.

Comparison of Yields between Crystallization- and Chromatography-Based Purification Platforms. At the completion of the crystallization process, the rAAV yield (i.e., percentage of the initial capsids that formed crystals) was calculated for the different experimental conditions at each pH (see Supplementary Figure 36). The corresponding average of the yields for each pH is shown in Figure 9. This suggests that

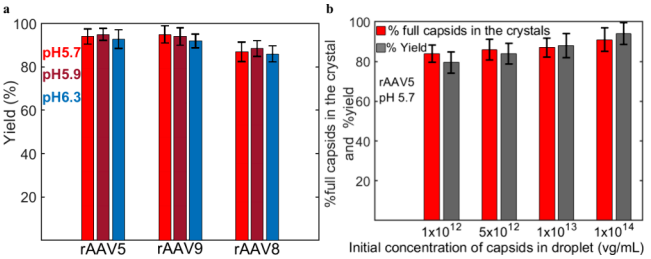

Figure 9. (a) Yields of preferential crystallization experiment at different pH for rAAV serotypes 5, 8, and 9. Starting concentration of capsids of 5 × 10^{13} vg/mL in a droplet. Error bar represents the mean and standard deviation of yields of preferential crystallization experiments performed at ≥4 crystallization conditions (as shown in Supplementary Figure 36) in the preferential crystallization region of full capsids of Sf9-produced rAAV. % Yield corresponding to each experimental condition as shown in Supplementary Figure 36 represents the mean from three experimental replicates with a standard deviation of 2.5%. Three analytical replicates of the ddPCR measurement (CBI, MIT) suggests that the variation in measurement is <1%. See Supplementary Figure 36 for experimental conditions. (b) Effect of initial concentration of capsids in a droplet on the purity/selectivity/enrichment of full capsids in the crystal and the yield of the preferential crystallization process for a starting sample with 51% rAAV5 full capsids. Error bars represent the mean and standard deviation from three experimental replicates. Preferential crystallization condition: 1.2 M NaCl, 3.3% PEG8000 at pH 5.7 (see rAAV Samples section in the Methods and Experiments section for detailed description on the production platform and purification methods used by the supplier).

the yield is consistently >88%, regardless of the pH and is weakly dependent on the serotypes. The yield of the preferential crystallization process is much higher than that obtained in single-cycle anion-exchange chromatography (AEX, 50−70%), cation-exchange chromatography (CEX, ∼80%), and UC-based purification (often ≪ 50%) and is comparable to the steric-exclusion chromatography (95%) and affinity chromatography (∼95%).[14,16,54,57,61,62] The concentration of capsids in both the crystals and the solution were calculated after the preferential crystallization and the total amounts of different capsids (full and empty) were compared with that before preferential crystallization. The results demonstrate that the total amounts of different capsids remained conserved after crystallization/purification process with <0.087% mass balance error.

Effect of Starting Concentration of Capsids on the Preferential Crystallization. Experiments were performed at lower starting concentrations of rAAV5 capsids in droplet to test if the preferential crystallization process is feasible/remains effective and to access the concentration dependency of the purity/selectivity and yield of the preferential crystallization process. The purity/selectivity (%enrichment of full capsids) shows a small decrease with decreasing initial concentration of capsids in the droplet (Figure 9b). A similar trend is observed

https://doi.org/10.1021/acsnano.5c00566
ACS Nano 2025, 19, 35348−35369

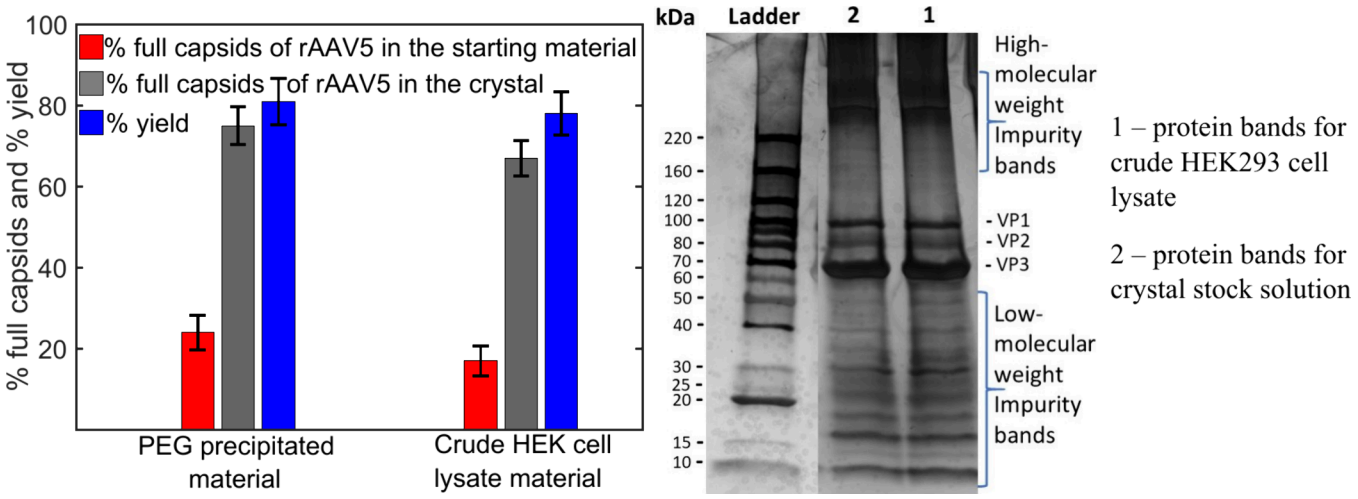

Figure 10. Left: Bar plots showing the enrichment of full capsids and yield after preferential crystallization from crude HEK293 cell lysate and from PEG-precipitated HEK293-produced capsids resuspension (resuspended in lysis buffer carrying the detergent as described in the rAAV Samples section in the Methods and Experiments section). Error bars represent the mean and standard deviation from three experimental replicates. Preferential crystallization condition: 1.5 M NaCl, 3.1% PEG8000 at pH 5.7. Right: SDS-PAGE analysis of the crude HEK293 cell lysate (1) and of the stock solution of crystals obtained after full capsids preferential crystallization from the crude HEK293 cell lysate (2). (See rAAV Samples section in the Methods and Experiments section for detailed description on the production platform and purification methods used by the supplier.).

for the yield of the preferential crystallization process. Both the yield and purity are higher than that obtained in the conventional purification methods across all concentrations examined. The results show that the preferential crystallization is feasible at initial concentrations of capsids lower than that used in the screening of crystallization conditions for construction of the phase diagrams. The preferential crystallization process is shown to be feasible in the more realistic concentrations (10^{12}–10^{13} vg/mL) typically encountered in commercial-scale production. Yield and full capsid enrichment for a capsid concentration lower than this could not be calculated, as no crystals were observed for capsid concentrations below 9×10^{11} vg/mL, which suggests that supersaturation was too low to nucleate crystals for the specific precipitant concentrations. This observation motivates the identification of a different set of precipitant concentrations from the phase diagram that favor the crystallization at capsid concentration below 9×10^{11} vg/mL. This is feasible as favorable crystallization conditions for low starting concentration of capsids can be created with a different set of precipitant concentrations as shown in Supplementary Figure 37. Alternatively, solution could be preconcentrated before carrying out the crystallization.

Effect of Extracellular and Intracellular Capsids and Detergents on the Outcome of Preferential Crystallization. During the production of rAAV, capsids are found both extracellularly and intracellularly, which typically requires cell lysis with detergents to release the viral particles. These intracellular and extracellular capsids copurify (as reported by Virovek), and thus, the samples provided by the Virovek contain both intracellular and extracellular capsids. All the preferential crystallization experiments preformed in this work are directly performed on the Virovek sample containing both the extracellular and intracellular capsids. Thus, the preferential crystallization method/protocol discussed in this work is applicable to both intracellular and extracellular capsids without any modification, and the method/protocol and the performance (purity and efficiency) of preferential crystallization for any intracellularly localized serotypes remain the same as that mentioned in this work.

As the gel electrophoresis (Figure 6) suggests, samples are partially purified samples, and the samples do not carry detergent (see rAAV Samples section in the Methods and Experiments section for detailed description of samples). Crystallization is a process driven by supersaturation, and for the crystallization to be successful, the concentration of the detergent must be much higher than its solubility (i.e., supersaturation). The concentrations of detergent, sodium lauryl sulfate, generally used in the cell lysis (0.1–1 w/v%) remain well below its solubility (1.5 w/v%) limit.[63,64] This implies that the detergent will not be crystallized along with the capsids, as the former's concentration remains well below its solubility. To further understand the effect of the detergents on the preferential crystallization process and its purity and efficiency, HEK293 cell-produced rAAV5 sample (PEG-precipitated sample in lysis buffer), which was prepared by PEG precipitation from the cell lysate followed by resuspension in the cell lysis buffer containing detergents as described in the rAAV Samples section in the Methods and Experiments section), was purchased from Virovek. The corresponding experimental result is shown in Figure 10. The data indicate that preferential crystallization is feasible in the presence of detergent, and both the selectivity/purity and yield of preferential crystallization process from the partially purified sample carrying detergents remain nearly the same as that obtained for partially purified sample without detergents (Figures 3 and 9, Table 1). This suggests that the detergent does not affect the preferential crystallization process. Thus, the preferential crystallization methos is applicable in a large-scale production, where the detergent used is typically part of the workflow.

Preferential Crystallization from Crude Cell Lysate. All the previous preferential crystallization experiments were performed from partially purified samples (see rAAV Samples section in the Methods and Experiments section for a detailed description of the samples). To understand whether the

https://doi.org/10.1021/acsnano.5c00566
ACS Nano 2025, 19, 35348–35369

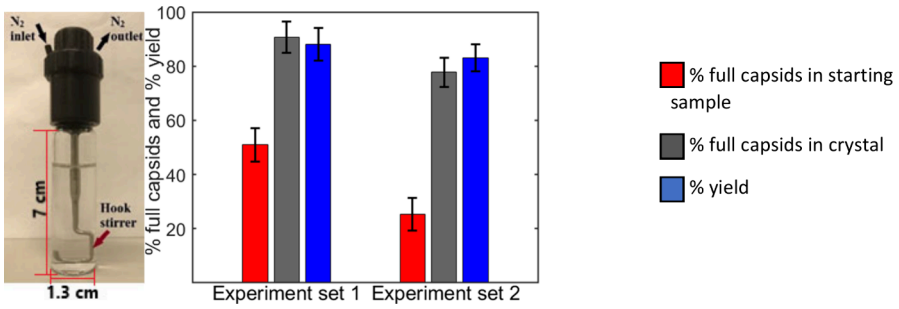

Figure 11. Preferential crystallization experiment in a scaled-up reactor (left) and the corresponding experimental result (right) showing the yield and enrichment/selectivity for preferential crystallization of full capsids of Sf9-produced rAAV5. Error bars represent the mean and the standard deviation from three experimental replicates. Experiment condition: 1.2 M NaCl, 3.5% PEG8000 at pH 5.7; Concentrations of rAAV5: 5×10^{12} vg/mL (2.5×10^{13} capsids or 0.25 mg capsid/batch for set 1) and 1×10^{13} vg/mL (7×10^{13} capsids or 0.7 mg capsid/batch for set 2). Batch volume: 5 mL (set 1) and 7 mL (set 2).

preferential crystallization is applicable to the crude cell lysate, which has not been passed through the affinity chromatography or PEG precipitation steps, additional experiments were performed. For this, a crude cell lysate sample from HEK293 suspension culture producing rAAV5 capsids was collected. The results in Figure 10 show that both the yield and the purity/enrichment of full capsids remain in the same range as that obtained for the partially purified samples (Figures 3 and 9 and Table 1). This shows that the preferential crystallization from the crude cell lysate is feasible without significantly affecting the yield and the selectivity/%enrichment of full capsids. SDS-PAGE analysis (Figure 10) shows that the preferentially purified capsids carry a significant amount of both low- and high-molecular-weight protein impurities form the crude cell lysate. This contrasts with the crystallization from the partially purified sample, where preferential crystallization effectively excludes the low molecular weight protein impurities from the crystals as shown in Figure 6. One explanation is that, in the crude cell lysate, the presence of high molecular weight protein impurities with low solubility may induce the coprecipitation of low molecular weight protein impurities with higher solubility. However, this needs a detailed analysis as the solubility is a strong function of precipitant concentrations. Identifying a separate set of precipitant concentrations from the phase diagram may suppress the precipitation of high and low molecular weight protein impurities while unaffecting the selectivity and yield. Thus, preferential crystallization from the crude cell lysate is feasible without significantly affecting the yield and the selectivity/%enrichment of full capsids irrespective of the level of the protein impurities.

Scale-Up of Preferential Crystallization Method. To determine whether preferential crystallization can be adapted to automated scaled-up crystallization device, experiments were performed in a 7 mL "crystallizer" (Crystalline, Technobis NL). Figure 11 shows the crystallizer and corresponding experimental results for rAAV5 for starting sample with 51% and ~15% full capsids. Results show that both the percentage of full capsids in the crystals and the yield are close to that found in hanging-drop experiment (Table 1 and Figure 9). These scale-up results suggest that the preferential crystallization observed in μL-volume droplet experiments is reproducible in a larger scale mL-volume reactor, and this approximately 10^4 times increase in the volume of the crystallization system does not affect the selective crystallization process, yield, and purity/selectivity of the full capsids. This supports the conclusion that the preferential crystallization is scalable. The conditions used for preferential crystallization experiment in a droplet or the 7 mL crystallizer can be used to perform preferential crystallization in crystallizers of any scale without further modification, as the thermodynamics of crystallization remain the same across scales.

STUDY LIMITATIONS

Though the preferential crystallization-based method presented here is applicable to any serotype of rAAV, and each serotype has its unique preferential crystallization region. These preferential crystallization regions are strongly dependent on the capsid surface structure/amino acid sequences. Thus, for each modified/engineered serotype, experimentation is necessary to determine the phase diagrams and the preferential crystallization regions specific to that modified/engineered capsid. Preferential crystallization regions can be dependent on the capsid production platform (e.g., Sf9 and HEK293) and the capsid's level of PTMs, which is influenced by the production platform as well as the downstream processing conditions (e.g., cell lysis conditions and downstream purification conditions). Thus, depending on the source of rAAV capsids, preferential crystallization conditions may vary. As the selectivity of the preferential crystallization process is dependent on the transgene length, the fraction of the partially filled capsids removed/rejected in the preferential crystallization process is limited to the fraction of capsids carrying transgene much smaller than the full capsids (wild-type capsids). This suggests that the preferentially crystallized full capsid crystals will still carry a small fraction of partially filled capsids. Because of the dependence of the selectivity on the transgene length, the fraction of capsids (overfilled capsids) carrying transgene of length larger than the full capsids will be cocrystallized with the full capsids and the resultant purified full capsids sample can carry some fraction of overfilled capsids.

CONCLUSIONS

Both the full capsid enrichment and yield achieved in preferential crystallization are greater than that reported for one round of conventional CEX-AEX (<75% full as observed in electron microscope image, 50−70% yield) and CEX-AEX-SEC (<75% full as observed in electron microscope mage, <50% yield).[54,58−60,67] AEX alone is only capable of a 50−70% yield with <65% full capsids from a starting sample with almost

https://doi.org/10.1021/acsnano.5c00566
ACS Nano 2025, 19, 35348−35369

15% full capsids.[14,54,68,69] Similarly, CEX alone is only capable of almost 80% yield with poor full capsid enrichment for a starting sample with low full capsids.[54,60] UC may approach 90% full capsid purity, but the recovery is often ≪50%.[16,62] Sequential isopycnic gradients are used to achieve higher full capsid enrichment, but at a substantial loss of recovered vector. In addition, copurifying impurities remain, which require additional process steps, e.g., SEC and dialysis, which further reduce yield. Scale-up results suggest that, starting with a low percentage of full capsids, two rounds of preferential crystallization can give a purity >95% with a recovery (yield) almost 80% (Figure 11). In contrast, two rounds of AEX would give almost 50% recovery and two rounds of UC would give a recovery of ≪25%.[16,62,68,69] Thus, the preferential crystallization method has the potential to be used in the downstream purification for removal of protein and salt impurities and enrichment of full rAAV capsids from cell lysate containing full, partially filled, and empty capsids and other protein impurities, in a single step, in one round, and, in a short period of time with full capsid enrichment, purity, and yield higher than the existing methods without the need of additional purification steps.

The product purity, concentration, scalability, and economics of crystallization explain why crystallization is a popular process for purification in small-molecule pharmaceutical manufacturing where crystallization processes are regularly scaled up from milliliters to 100s to 1000s of liters.[65] Crystallization equipment does not require any resin or specialized equipment or expensive chromatography media. Importantly, to produce high-quality, e.g., clinical grade rAAV, would involve single-use components, which greatly increases the production costs. Crystallization usually involves standard stirred tanks, which is the lowest cost equipment in any manufacturing facility, many orders of magnitude lower than chromatography columns, which often consists of specialized resigns or columns.[66] This inflates the cost of scale up for the chromatography-based protein purification method to be many folds higher than that of crystallization-based method. The stirred tanks used for crystallization can be run with no to minimal maintenance for decades.[65] Thus, preferential crystallization-based method will facilitate the large-scale production of rAAV.

METHODS AND EXPERIMENTS

Materials. All chemicals used in the experiments were of molecular biology grade. Sodium dihydrogen phosphate dihydrate (BioUltra, ≥99.0%), sodium hydroxide (BioXtra, ≥98% anhydrous), 1 M hydrochloric acid (BioReagent, for cell culture), sodium chloride (BioXtra, ≥99.5%), potassium chloride (BioXtra, ≥99.5%), potassium dihydrogen phosphate (BioUltra, ≥99.5%), phosphate-buffered saline (PBS 1X (150 mM sodium phosphate and 150 mM NaCl), pH 7.2; BioUltra solution), polyethylene glycol (PEG-8000, BioUltra; PEG-6000, BioUltra), phosphotungstic acid (10% solution), and propidium iodide solution (1 mg/mL in water) were purchased from Sigma-Aldrich. Dulbecco's 1X PBS, FreeStyle 293 F cells, FreeStyle 293 expression medium, DMEM 1X (Dulbecco's modified Eagle medium), and 0.25% trypsin-EDTA (1X), FBS (fetal bovine serum) were purchased from Thermo Fisher Scientific. Nuclease-free water (Ambion nuclease-free water), Trypan blue stain (0.4%), and Countess II automated counting slides were purchased from Invitrogen. Poloxamer-188 (Pluronic F-68, 10%, BioReagent) was added to rAAV-containing solutions at 0.001% to suppress binding to container surfaces. Glutaraldehyde solution (10% aqueous solution) and copper grid (carbon support film, 200 mesh, Cu; CF200-CU-50) were purchased from Electron Microscopy Sciences. Amicon Ultra centrifugal filter (10 kDa, UFC5010) and Ultrafree MC VV centrifugal filters (PVDF 0.1 μm; UFC30VV25) were purchased from Millipore Sigma. Falcon tube (5 mL, polystyrene round-bottom tube with cell-strainer cap), cell culture dish (10 cm × 2 cm), Erlenmeyer shake flask (125 mL), Costar 96-well cell culture plate (TC treated, sterile), and 6-well cell culture plate (TC treated, sterile) were purchased from Corning. ELISA kits were purchased from Progen and stored in a 4 °C refrigerator. DNA primers were purchased from Integrated DNA Technologies (Coralville, IA, USA). Eva Green Supermix was purchased from Bio-Rad Laboratories. The cover glasses and the silicon gaskets containing six sample wells for mass photometry measurement were provided by Refeyn Ltd. (MA, USA).

rAAV Samples. Recombinant adeno-associated virus serotypes, rAAV5, rAAV8, and rAAV9, both as full (genome-loaded) and empty (without genome) capsids, were purchased from Virovek at a reported concentration of 10^{14} vg/mL. The sample labeled as "full rAAV5" (Lot 19−047E) from Virovek actually contains 80% full and 20% empty capsids, and the sample labeled as "empty rAAV5" (Lot 19−253E) from Virovek contains 92% empty and 8% full capsids and was purified using ultracentrifugation (as reported by Virovek). The "full rAAV8" sample actually contains 80% full and 20% empty capsids, and the "empty rAAV8" sample actually contains 96% empty and 4% full capsids and was purified using ultracentrifugation. Similarly, the sample labeled as "full rAAV9" (Lot 21−100) from Virovek contains 80% full and 20% empty capsids, and the sample labeled as "empty rAAV9" (Lot 21−077) contains 96% empty and 4% full capsids and was purified using ultracentrifugation. Unless mentioned, the full rAAV capsids contained a genome of length 2.46 kbp with cytomegalovirus (CMV) promoter expressing green fluorescent protein (GFP). Virovek quantified the full and empty capsids using qPCR and nanodrop OD (optical density) measurement. In-house quantification of full and empty capsids using ddPCR and ELISA produced roughly similar results as reported by Virovek. Virovek uses proprietary methods for cell lysis as well as downstream purification. As per Virovek, cell lysis was performed using a proprietary lysis buffer and surfactant sodium lauryl sulfate to break open the vectors. For Sf9-produced rAAV5, rAAV8, and rAAV9 capsid samples in Figures 2, 7, and 8, multiple rounds of ultracentrifugation were used post lysis and represent the highly purified and concentrated samples. Sf9-produced rAAV5, rAAV8, and rAAV9 capsid samples in Tables 1 and 2 and Figures 5, 6a, 9, and 11 were postlysis affinity chromatography purified samples, which, on SDS-PAGE analysis, showed the presence of low-molecular weight protein impurities and were thus partially purified samples. Sf9-produced rAAV5 samples carrying 4.68 and 1.2 kbp transgene in Figure 4a were PEG precipitated and resuspended in PBS buffer and were thus partially purified samples. Samples for mass photometry experiment in Figure 4b were ultracentrifugation purified samples carrying a significant fraction of full, empty, partially filled, and overfilled capsids and were highly purified samples. AAV5 samples for studying PTMS effect in the Figure 3 were produced in two different systems, HEK293 and Sf9, but were purified using the same protocol, which includes PEG precipitation from cell lysate and resuspension in PBS buffer, which removes detergent and partially removes the cell debris and protein impurities. The sample for studying the effect of crude cell lysate in Figure 10 was HEK293-produced rAAV5, and cell lysis was performed using a detergent. This sample was unpurified and included all the cell lysis materials and impurities in it. Samples for studying the effect of detergent in Figure 10 were PEG-precipitated HEK293-produced rAAV5 capsids, where cell lysate was PEG precipitated and then resuspended in PBS buffer containing lysis detergent. This sample carried part of the protein impurities from cell lysis and was thus partially purified. SDS-PAGE analysis of Virovek samples (Figure 6) suggests that the affinity purified samples and PEG precipitated samples carry a significant amount of low-molecular-weight protein impurities from the cell lysis. Thus, some of the Virovek samples are partially purified samples as suggested by our SDS-PAGE analysis. For each type of sample, Virovek supplied the sample from the same batch, so the rAAV samples in our experiments do not have the variability that can occur

https://doi.org/10.1021/acsnano.5c00566
ACS Nano 2025, 19, 35348−35369

when samples are taken from different batches. rAAV samples were supplied at a pH of 7.2 in PBS buffer in small vials holding 100 μL samples each and were stored long-term at −80 °C. Before putting the samples into the freezer, 100 μL sample from each vial was divided into 5 equal aliquots. Aliquots are stored at −80 °C for long-term use. For short-term use, based on requirement, small vials were taken out of the −80 °C freezer and stored at 4 °C, at which AAV is stable for 4 weeks.[70,71] All the capsid samples purchased from the Virovek include both extracellular and intracellular rAAV particles. During the production of rAAVs, some rAAVs are primarily found intracellularly and others are primarily found extracellularly. Intracellular rAAVs are cracked open from the host cell by cell lysis with detergent. Then the intracellular and extracellular rAAV capsids are copurified from the cell lysis material using the methods described earlier. Preferential crystallization experiments were performed directly on the Virovek samples without separating/differentiating intracellular and extracellular capsids. Therefore, the crystallization method/protocol described in this Article are applicable to both the intracellular and extracellular capsids.

Hanging-Drop Vapor-Diffusion Experiment. Crystallization conditions for rAAVs are screened in a hanging-drop vapor-diffusion experiment (Supplementary Figure 3) using VDX 24-well crystallization plates (cat no. HR3−141, HR3−108, 306) with glass coverslips on top (Hampton Research, California, USA).[35,72] Each well contains two liquid solutions: one being a droplet of small volume of 2 μL suspended from a hydrophobic glass coverslip (Hampton research, California, USA) at the top of the well and the other being a reservoir of 1 mL at the bottom of the well. Each drop and reservoir contain polyethylene glycol (PEG) 8000 and sodium chloride (NaCl) as precipitants dissolved in a phosphate-buffered saline (PBS) solution. PEG8000 is tested because it has been used in the past literature for the crystallization of rAAV.[73] The reservoir is to ensure the controlled evaporation from the droplet (Supplementary Figure 3).

Each droplet was a mixture of 1 μL of AAV sample and 1 μL of buffer solution containing PEG and salt. Initial screenings were performed by varying the concentration of PEG8000 (from 0.1 to 7 w/v%) with a constant NaCl concentration. Subsequent screenings were conducted by varying the NaCl concentration (0 to 2.4 M) to fine-tune the ionic strength of the crystallization medium. As time progresses, water evaporates from the droplet. Some time after supersaturation is reached, the nucleation of capsid crystals begins, and eventually, the evaporation rate slows down (due to the reduction in vapor pressure driving force), at which point no further reduction in the volume of the droplet takes place.

Each droplet was monitored at regular intervals for a period of 1 to 2 weeks via an optical microscope (Imaging Source DMK42BUC03) to track the evolution of crystals. The particles are observed in real time using a microscope with an in-built CCD camera (Leica Z16 APO), using both normal and polarized light. Depending on the experimental condition, nucleation of capsids may begin a few hours to 2 weeks after the beginning of experiment and nucleation may take a few hours to a day to complete, which was followed by growth of the crystals for up to 2 to 3 days; at which point no further change in the crystals was observed. All experiments are performed for pH between pH 5.5 to 8.5 where the rAAV particles are stable (low degradation).[71,74] All experiments were performed at room temperature, 23 ± 2 °C.

To study whether the preferential crystallization method is feasible if PEG with molecular weight other than PEG8000 is used, we explored PEG with molecular weight of 6000. The role of PEG in crystallization process is to create the volume exclusion effect in the solution to produce the supersaturation necessary for the crystallization to occur.[32,33] Depending on the molecular weights (types) of PEG, this level of supersaturation will be higher or lower concentration, but irrespective of molecular weights, each type of PEG will result in preferential crystallization region.

Construction of Phase Diagram. To find crystallization conditions (i.e., the concentration of precipitants PEG and NaCl at a specific pH), where only either full or empty capsids are crystallized, >500 crystallization conditions are screened for "full" capsids and "empty" capsids samples each for specified values of the pH. At each tested condition, the AAV capsids either remain in solution, form an amorphous precipitate, or form crystals. A phase diagram is then constructed/formed/prepared by plotting these outcomes/data as a function of PEG and NaCl concentrations. Separate phase diagrams are determined for "full" and "empty" capsids samples at different pH values (Supplementary Figure 8). To screen 500 crystallization conditions, the whole parameter space is discretized into different regions, where each region represents an experimental condition as shown in Supplementary Figure 4. This approach allows exploring one parameter at a time while keeping other parameters constant. Based on the outcome of an experiment, the next experiment is performed at higher concentration (higher spacing) or lower concentration (lower spacing). Please visit Supplementary Figure 4 for exemplary phase diagrams and corresponding experimental points.

Crystallinity Confirmation. X-ray diffraction (XRD) is the most commonly used method to confirm the crystallinity of a material.[72,75−77] Single crystal X-ray diffraction was performed with crystals looped out from the droplet, but because of the extremely high molecular weight and resulting dense structure, it was not successful. All the previous X-ray diffraction studies involving rAAV crystals used high energy synchrotron X-rays, which are not accessible for regular use.[73,77,78] Because XRD requires a relatively large sample mass (∼0.2 g), for limited samples, crystallinity is determined by an alternative method, cross-polarized light microscopy, which does not depend on the quantity of the sample.[79,80]

Polarization Study. The optical properties of the crystals are assessed using normal and cross-polarized light microscopy.[80,81] Screening of crystallization conditions based on birefringence in cross-polarized light microscope is much simpler and faster than destructive methods such as SEM and TEM, making the approach suitable for repetitive screening of a large number of conditions. Crystals appear as colorless or gray in normal light microscopy images (Supplementary Figure 12a) and show birefringence in cross-polarized light (Supplementary Figures 12b and 13). For analysis in cross-polarized light microscopy, a 24-well plate was positioned on a cross-polarized light microscope (Leica Z16 APO) base, and each droplet was observed. Then, plane-polarized light, which is coming from the base polarizer, is passed through the crystals, and the analyzer, which is also a polarizer, is rotated 360° while keeping the crystal's position fixed. On rotation of the analyzer, anisotropic crystals will assume a spectrum of interference color except at every 90° position of the analyzer (with respect to the base polarizer), where the interference is extinct and the crystals appear dark/extinct (Supplementary Figure 13). This phenomenon is known as birefringence and confirms the crystallinity of particles.[81]

When crystals are observed under cross-polarized light, crystals remain dark/extinct (Supplementary Figure 13) at every 90° position (where two polarizers' vibration directions are perpendicular to each other) and show interference coloration on rotation due to the splitting of the transmitted light into two rays: slow (e) and fast moving (o) rays.[81−83] These photos (Supplementary Figure 13) indicate that the crystals are optically anisotropic (i.e., the speed of light varies with direction) and birefringent (i.e., depends on the polarization and propagation direction of light).[81,84] The presence of a unique angle of extinction and birefringence in the crystals in this analysis suggests that the particles are single crystals, in contrast to polycrystalline materials which would appear isotropic.[84,85] Under cross-polarized light, isotropic crystals do not show any birefringence as light passes through without splitting, and the crystals appear dark (extinct) because of the absence of interference.[84] Similarly, materials that are not crystals (e.g., protein aggregates) do not show any birefringence.[84] The literature suggests that NaCl generally forms cubic crystals (isotropic) and does not show any interference colors under cross-polarized light microscope.[83,84] Thus, rAAV crystals can be easily distinguished from NaCl crystals if NaCl is present in the system. All AAV capsid crystal particles generated in this study are optically anisotropic and are not cubic in shape, which indicate that the particles are not NaCl crystals.

https://doi.org/10.1021/acsnano.5c00566
ACS Nano 2025, 19, 35348−35369

Stock Solution Preparation: Crystal Collection, Dissolution, and Stock Solution Preparation for Biological Analysis (ELISA, ddPCR, Cell Infection, Flow Cytometry, SDS PAGE, Mass Photometry). For biological assays, rAAV stock solution is prepared by dissolving crystals. To prepare AAV stock solution, a droplet containing well-developed crystals is viewed under normal optical microscope, and the droplet is diluted with equal volumes (5 μL each) of reservoir solution and 1X PBS buffer solution (pH 7.2) to prevent the dissolution of crystals. Then, the crystals are detached from the glass surface by careful rubbing with the micropipette tip to avoid the breakage of the crystals, collected into a centrifugal filter of 0.1 μm pore size (Millipore Sigma), and centrifuged once at 200g for 1 min at room temperature. The crystals remain attached to the filter paper, effectively removing free AAV particles, PEG, and NaCl that remain in the supernatant. Based on the crystal size, the pore size of the filter paper is changed. The crystals are washed twice (100 μL of 1:1 mixture of reservoir solution and 1X PBS) to ensure the complete removal of residual virus capsids and to dilute the PEG and NaCl. The number of washing steps may vary based on the type of crystals in the droplet as AAV crystals are very soft and prone to breakage even with low shear. For small crystals, 1/2 washing steps were performed to avoid breakage and eventual passage of crystals through the filter membrane pores. Then, the crystals are washed once with 100 μL of diH_2O ($\geq$18 mΩ, Milli-Q) and centrifuged at 200g for 1 min to remove the adsorbed PEG and NaCl from the filter. The centrifugation is performed immediately after addition of diH_2O as crystals are highly soluble in water. The AAV crystals are then dissolved in 300 μL of nuclease-free water in 4 °C refrigeration for 30 min. The dissolved crystal solution is transferred into an Amicon centrifugal filter (10 kDa NMWCO) and centrifuged at 10000g for 5 min. Capsids are then washed 3 times using 200 μL of nuclease-free water at 10000g for 5 min each time to ensure complete removal of remaining salt and precipitant. The capsid particles are then resuspended into 200 μL of Dulbecco's 1X PBS (DPBS without magnesium and calcium) and collected into a vial and stored at 4 °C for short-term use. For long-term storage, 5% sorbitol solution is added to the capsid suspension and stored in a cryovial at −80 °C.[86]

Calculation of Percentage of Full and Empty Capsids in Crystals. *ELISA Experiment.* ELISA assay protocols followed the manufacturer's instructions (Progen) for rAAV5 (AAV5 Xpress ELISA kit), rAAV8 (AAV8 Xpress ELISA kit), and AAV9 (AAV9 Xpress ELISA kit).[87−89] Briefly, to determine a workable capsid concentration for ELISA assays, a range of concentrations is produced by serial 2-fold dilution of the AAV stock solution (see section for stock solution preparation): 1:2, 1:4, 1:8, 1:16, 1:32, 1:64, 1:128, 1:256, 1:512, 1:1024. Capsid concentrations outside the workable range will either lead to signal saturation or low signal when the concentration is too high or too low, respectively. Assay buffer (ASSB 20X) as provided by the manufacturer (Progen) is diluted to ASSB 1X using diH_2O (Milli-Q). Similarly, (lyophilized) capsid standards (Progen), known as 'kit control' (KC), are included in the ELISA kits. The KC is reconstituted using ASSB 1X (500 μL) and a serial dilution (1:2, 1:4, 1:8, 1:16, 1:32, 1:64) is prepared using ASSB 1X. Anti-AAV mAb-biotin conjugate is dissolved in ASSB 1X (750 μL) to produce 20X biotin solution. The assay is performed following the procedure as recommended by the ELISA kit manufacturer. For both KC dilution and sample dilution, duplicates are prepared. Undiluted KC is used as a control. KC dilution (100 μL) and AAV stock dilution (100 μL) are loaded on ELISA plate and incubated (37 °C for 20 min). After 20 min, solution from each well in ELISA plate is aspirated off and washed (3x 100 μL ASSB 1X buffer in each well). 100 μL of the biotin 1X solution is aspirated into each well and incubated (37 °C for 20 min). Plate is then removed and washed as before. 100 μL 1X Strep HRP solution is aspirated into each well and incubated (37 °C for 20 min). Then, 100 μL of TMB (tetramethyl benzidine) was aspirated into each well and incubated (37 °C for 20 min). The solution in some of the well turns blue, which is stopped using 100 μL of stop solution (Progen kit). Solution in some well turns yellow indicating the cease of reaction. Immediately, the plate was taken for reading in a microplate reader (Synergy H1; BioTek Instruments, Winooski, VT, USA) at 450 nm wavelength. Absorbance readings for the sample dilution as well as KC dilution are corrected by subtracting the absorbance of the control. The averaged absorbance values, from duplicates, for the KC dilution (along the *y*-axis) are plotted against the corresponding concentration along the *x*-axis, and a 4-parameter logistic (4PL) fit is performed in Matlab to calculate the concentration of the capsids in the sample.

ddPCR Assay. The quantity (i.e., titer) of genomes is determined using ddPCR assays. The protocol is adapted from the method as described in BIORAD and Tam et al.[90,91] Like ELISA, a serial dilution (1:2, 1:4, 1:8, 1:16, 1:32, 1:64, 1:128, 1:256, 1:512, 1:1024) of AAV stock solution (see Section for stock solution preparation) was performed using DNase-free water (Thermo Fisher Scientific). A master mix solution (18.2 μL for each well) is prepared by mixing 7.79 μL of 2.62% DMSO (Thermo Fisher Scientific), 0.41 μL of primer mix (forward and reverse; BIORAD), and 10 μL of EvaGreen Supermix (QX200 ddPCR EvaGreen Supermix; BIORAD). In each well of the 96-well PCR plate (ddPCR plates 96-well, semi-skirted), diluted AAV stock solution (2.2 μL, containing DNA template) and the master mix (18.2 μL) are combined to make a total of volume of 20.4 μL, the plate is sealed in a PCR plate sealer (PX1, BIO-RAD, California, USA), and the contents of the solution in each well were spun down by centrifuging (1 min 1500 rcf; centrifuge 5910R Eppendorf). For each dilution, a duplicate sample is prepared. The PCR plate is then transferred to a droplet generator (Automated droplet generator, BIO-RAD, California, USA). After generation of droplets, the PCR plate is placed into a thermal cycler (CFX96 deep well real time system; C1000 touch; BIO-RAD, California, USA) for the PCR reaction to take place for amplification of the DNA. The standard thermal cycles used for PCR reaction (as set by BIO-RAD) are 1 cycle of an enzyme activation step (95 °C for 5 min) and 40 cycles of an amplification cycle consisting of denaturation (95 °C for 30 s), and annealing/extension (60 °C for 1 min). Following the amplification cycles, a signal stabilization cycle, is performed (4 °C for 5 min for 1 cycle and then at 90 °C for 5 min). Finally, sample is held at 4 °C before being removed from cycler. Primers used targeted the GFP sequence. Forward primer was 5'-GCAAAGACCCCAACG-AGAAG-3', and reverse primer was 5'-TCACGAACTCCAGCA-GGACC-3'.

After completion of PCR reaction, the PCR plate is inserted into a PCR droplet reader (QX200 Droplet reader, BIO-RAD, California, USA). PCR plate reader reports the number of copies of DNA per μL in each dilution. Then average value of DNA copies per μL is calculated for each duplicate set of dilution. Number of DNA copies in the stock solution and in the crystals are calculated back.

Room Temperature TEM Analysis of rAAV Particles after Crystallization. To visualize and measure the percentage of full and empty capsids in the crystals as well as to understand whether the virus particle's morphology remains the same, room temperature TEM imaging is per-formed. The droplet containing crystals is viewed under normal optical microscope and the droplet is diluted with equal volumes (5 μL each) of reservoir solution and 1X PBS buffer solution (pH 7.2) to prevent the dissolution of crystals. Then the crystals are detached from the glass surface, aspirated and dispensed on a centrifugal filter of 0.1 μm pore size (Millipore Sigma) and centrifuged once at 200g for 1 min to remove the free capsids and solution. The AAV crystals are then dissolved by adding diH_2O (100 μL) onto the filter (30 min at room temperature). The solubilized capsids are fixed by adding 2.5% aqueous glutaraldehyde solution in 1:1000 v/v ratio to inactivate the capsids.

Virus particles images are obtained by TEM (JEOL 2100 FEG model) at room temperature (TEM facility, Koch Institute, MIT). For sample preparation, a protocol developed by the MIT Koch Institute was adapted. To briefly describe, a 10 μL of dissolved crystal solution is aspirated and dropped on a 200-mesh copper grid coated with continuous carbon film (EMS) at room temperature. After 10 min, any remaining water on the grid is absorbed by a tissue paper (Kim wipes) and 10 μL of 1% aqueous phospho-tungstic acid solution is immediately dropped onto the moist TEM grid. After 30 s, the excess liquid is absorbed by a tissue paper. The grid is left at room

https://doi.org/10.1021/acsnano.5c00566
ACS Nano 2025, 19, 35348−35369

temperature for 45 min to allow the remaining liquid to dry before inserting the grid into the TEM chamber. Standard operation procedure as developed by JEOL is followed to operate the TEM equipment. All images are captured using minimum dose method that, were essential to avoid sample damage under the electron beam. The microscope was operated at 200 kV and with a magnification in the ranges of 10,000 ∼ 60,000 for assessing particle size and distribution and recorded on a Gatan 2k × 2k UltraScan CCD camera. Empty capsids show the contrast difference as shown in the Supplementary Figures 18a-l.[92] The heavy metal stain is taken up by the empty capsids which diffracts the electron beam appearing as black areas (Supplementary Figure 18, black arrows) in the image whereas full capsids exclude the heavy metal atoms and appear as uniformly shaded hexagons (Supplementary Figure 18, white arrows).

Mass Photometry Experiment. Mass photometry measurements are performed in a SamuxMP instru-ment (Refeyn Ltd., MA, USA), which has a higher resolution tailored especially for AAV vector analysis. A protocol developed by the Refeyn Ltd. (MA, USA) as described in Wu et al. was adapted.[93] Mass photometry is based on interferometric scattering, where the intensity of the interference pattern/contrast between the scattered light from the particle and the reflected light from the glass surface is measured and the intensity is proportional to the mass of the particle. The calculated masses of individual particles are plotted as a histogram and each peak in the histogram represents a distinct subpopulation of the particles with a specific mass. To obtain the correlation between the mass and contrast signal, prior to each measurement, a calibration is performed using "empty" AAV9 vector of known mass of 3.74 MDa and having the same refractive index as that of capsids in the sample. The molar mass of the "empty" AAV9 is provided by Refeyn Ltd. (MA, USA). To briefly describe the experiment, 10 μL of 1X PBS is pipetted into a well of silicon gasket, the focus is adjusted automatically, and then 10 μL of AAV9 calibrant is added into the loaded PBS. Before measurement, the loaded sample and PBS are mixed vigorously by aspirating and dispensing multiple times carefully to avoid formation of bubbles. The measurement time is set to 60 s, which captures the binding and unbinding events in the form of a movie. The measurements are recorded using Acquire MP 2.4.2 (Refeyn Ltd., MA, USA) and analyzed with Discover-MP (v2023 R1.2) (Refeyn Ltd., MA, USA). For all the measurements, the binning width is set to 40, and the ratiometric contrast distribution is fitted by a Gaussian function to obtain the molecular weight of subpopulation. The F/E ratio (full capsid to empty capsid ratio) and linearity are visualized using MATLAB.

Capsid Protein Sequencing and PTMS (Post-Translational Modification) Analysis Using LC-MS. For mass spectrometry analysis, protein is first digested overnight, passed through a chromatography column, and analyzed in Thermo Orbitrap Exploris 480 mass spectrometer (Thermo Fisher Scientific). For protein digestion, a protocol developed by Protifi (NY, USA) is adapted.[94] 25 μg of the rAAV capsid sample is reduced with 10 mM DTT (final concentration) at 95 °C for 10 min, and the disulfides are alkylated with 20 mM iodoacetamide (final concentration) at room temperature for 30 min in a dark room. Then S-trap micros (spin column; Protifi) and phosphoric acid (final concentration 2.5%) are added into the sample and maintained a pH of <1 and vortexed. 165 μL of binding buffer is added, and the S-trap micros are transferred into a centrifuge tube and centrifuged (4,000g for 30 s) to trap proteins and washed with wash buffer (3x 100 μL at 4,000g for 30 s). The protein is then digested with 20 μL of digestion buffer containing trypsin (1:10 wt ratio) by incubating at 47 °C for 2 h and eluted with elution buffer 1 (50 mM TEAB in water), elution buffer 2 (0.2% formic acid in water), and elution buffer 3 (50% acetonitrile in water) following the procedure as suggested by Protifi (NY, USA).

The tryptic peptides were separated by reverse phase HPLC (Thermo Ultimate 3000) using a Thermo PepMap RSLC C18 column (2 μm tip, 75 μm × 50 cm PN# ES903) over a 90 min gradient before nanoelectrospray using a Orbitrap Exploris 480 mass spectrometer. Solvent A was 0.1% formic acid in water, and solvent B was 0.1% formic acid in acetonitrile. The gradient conditions were 1% B (0−10 min at 300 nL/min), 1% B (10−15 min, 300 nL/min to 200 nL/min), 1−7% B (15−20 min, 200 nL/min), 7−25% B (20−54.8 min, 200 nL/min), 25−36 B (54.8−65 min, 200 nL/min), 36−80% B (65−65.5 min, 200 nL/min), 80% B (65.5−70 min, 200 nL/min), 80−81% B (70.0−70.1 min, 200 nL/min), 1% B (70.1−90 min, 200 nL/min). The Thermo Orbitrap Exploris 480 mass spectrometer was operated in a data-dependent mode. The parameters for the full scan MS were resolution of 120,000 across 375−1600 m/z and maximum IT 25 ms. The full MS scan was followed by MS/MS for as many precursor ions in a two second cycle with a NCE of 28, dynamic exclusion of 20 s, and resolution of 30,000.

Raw mass spectral data files (.raw) were searched using Sequest HT in Proteome Discoverer (Thermo) with the following search parameters: 10 ppm mass tolerance for precursor ions; 0.02 Da for fragment-ion mass tolerance; 2 missed cleavages of trypsin. Depending on the sample the data was searched against a Human(uniport), *Spodoptera frugiperda* (uniport), AAV8(uniport), AAV9(uniport) and a contaminates database (made in house). Following post-translational modifications were searched for: Carbamidomethylation (Cys), Oxidation (Met), Phosphorylation (Ser,Thr,Tyr), Sumoylation by Sumo-1 (Lys), Sumoylation by Sumo-2/3 (Lys), Acetylation (Lys/His), Ubiquitination (Lys), Methionine loss at the N-terminus of the protein, Acetylation of the N-terminus of the protein, Met-loss plus acetylation of the protein N-terminus.

Crystal Purity Analysis. *SDS-PAGE Electrophoresis Analysis of Capsid Proteins.* SDS-PAGE analysis is performed to assess the quality of the AAV samples and determine whether crystallization affects the viral protein integrity. For electrophoretic resolution of capsid proteins, protocols described by Oyama et al., 2021, Zhou et al., 2025, and BIORAD were adapted.[95−97] Viral proteins are first denatured and reduced by incubating a mixture of AAV sample, 2-mercapto-ethanol (along with SDS, dye and glycerol), and diH_2O (2:1:2 volume ratio) at 95 °C for 10 min.[97] The denatured samples and the protein ladder (BenchMarkTM, Thermofisher) are loaded and resolved electrophoretically through a 4−20% polyacrylamide gel (BIO RAD TGX gradient gel) in a Mini-PROTEAN tetra electrophoresis cell/chamber in 1X Tris/glycine/SDS buffer at 100 V for 100 min. Then, the gel is either treated with silver staining agent or Coomassie blue staining agent. For silver staining, a protocol as described in the Silver Stain Plus kit (BIORAD) is followed.[98] As per the instruction, the following reagents are prepared: fixative enhancer solution (a mixture of 100 mL reagent-grade methanol, 10 mL reagent-grade acetic acid, 20 mL fixative enhancer concentrate as provided by BIORAD, and 60 mL diH_2O), development accelerator solution (a mixture of 50 mL diH_2O and 3 g of development accelerator reagent as provided by BIORAD), silver staining solution (diH_2O, silver complex solution, reduction moderator solution, and image development solution in the volume ratio 7:1:1:1), and stop solution (5% acetic acid solution). Then, the gel is treated as per manufacturer's instruction (BIO RAD),[98] except the final Ag staining step, where the gel is stained for only 7−10 min. To briefly describe the procedure, the gel with the resolved proteins after the electrophoresis is treated with the fixative enhancer solution under gentle agitation for 20 min and then rinsed with diH_2O (3 × 200 mL). The gel is then placed in a staining and developing solution (development accelerator solution and silver staining solution in volume ratio 10:7) for 7−10 min, and then, staining is stopped using stop solution. The silver-stained gel is imaged in the ChemiDoc imaging system (BIORAD). For Coomassie blue staining, the gel is stained as per the manufacturer's instruction (Invitro-gen SimplyBlue Safe Stain protocol).[99] To briefly describe the procedure, after electrophoresis, the gel is rinsed with diH_2O (3 × 200 mL) and then stained with 20 mL of SimplyBlue Safe Stain. The gel is then rinsed again with diH_2O (2 × 200 mL) and imaged in ChemiDoc imaging system for analysis.

Western Blot. AAV sample is denatured and resolved electrophoretically following the procedure as described for SDS-PAGE analysis. Blotting and antibody application procedure are adapted from the Western blot protocol developed by ABCAM.[100] After electrophoretic resolution, the protein is transferred (blotted) from

https://doi.org/10.1021/acsnano.5c00566
ACS Nano 2025, 19, 35348−35369

gel to polyvinylidene fluoride (PVDF) membrane using wet transfer method in a tank in 1X Tris-glycine buffer at 100 V for 100 min following the procedure as described by ABCAM. For antibody application, Anti-AAV VP1/VP2/VP3Mouse monoclonal, B1 primary antibody (Progen Biotech), Rabbit Anti-Mouse IgG H&L (HRP) secondary antibody (ABCAM), and SuperSignal Western Blot Enhancer (Invitrogen) are purchased. To briefly describe the procedure, after blotting of protein, the membrane is covered with a blocking buffer (5% nonfat dry milk in 1X TBST) and incubated overnight in a container with gentle rocking at 4 °C. Then, the membrane is rinsed with wash buffer (20 mLx3 TBST for 10 min each) and covered with primary antibody in blocking buffer (1 μL primary antibody in 50 mL of 2% nonfat dry milk in 1X TBST) and incubated at room temperature for 1.5 h under gentle rocking. Membrane is then washed again with wash buffer (20 mLx3 TBST for 10 min each) and covered with the secondary antibody in blocking buffer (1 μL secondary antibody in 50 mL of 2% nonfat dry milk in 1X TBST) and incubated at room temperature for 1.5 h under gentle rocking. The membrane is then washed again (20 mL × 3 TBST for 10 min each) and covered with 1 mL of SuperSignal Western Blot Enhancer solution and imaged in ChemiDoc imaging system.

EDAX (Energy Dispersive X-ray) Analysis. EDAX analysis of crystals is performed in an Octane Elect Super Detector (EDAX, AMETEK materials analysis division, NJ) attached with a SEM microscope (ZEISS Merlin, MIT Material Science) in an electron microscope facility at Koch Institute, MIT. For EDAX analysis of rAAV crystals, conditions that produce well-developed crystals with sharp edges are considered. The droplet is diluted with equal volumes (5 μL each) of reservoir solution and 1X PBS buffer solution (pH 7.2) to prevent the dissolution of crystals and facilitate manipulations. The solution is agitated carefully to detach the crystals from glass surface without breaking the crystal. Then the crystals and solution are aspirated and dispensed on a centrifugal filter of 0.1 μm pore size (Millipore Sigma) and centrifuged once at 2000g for 1 min to remove the free capsids and solution. Then, the membrane filter paper is cut out of the tube frame and attached on a carbon tape on a brass stub and mounted on the SEM chamber. EDAX analysis is performed following the standard software-based operating procedure as described by the AMTEK.[101−103] To briefly describe, for EDAX analysis, a crystal is first selected on the membrane surface ,and then, elemental mapping is done on a selected area, which includes both the crystal and the underlying membrane surface. Elemental mapping of the membrane surface serves as a control. Finally, point EDAX analysis is performed on the crystal at different points to obtain the elemental compositions of the crystal at those points, and the average elemental composition of the crystal is calculated by athematic averaging.[102,103] For all of the analysis, more than 100 scans are used unless mentioned. Crystals analyzed in EDAX are more than 10 μm thick and a beam of 15 kV is used for this analysis.

Cell Biological Activity Measurement. *Preparation of Adherent Cell Culture.* To determine whether crystallization affects biological activity of rAAV, HEK293 T cells are transduced. The cryopreserved HEK293 T (ATCC) cells are thawed (2 min at 37 °C water bath) and transferred into a centrifuge tube that contains 9 mL of complete growth medium (10 v/v% FBS in DMEM; Thermo Fisher Scientific). The cells are then pelleted (centrifuged at 1000g for 5 min) and resuspended in complete growth medium. This process is repeated three times to remove the DMSO used in cryopreservation. The cell pellet is then resuspended in the preconditioned complete growth medium (9 mL at 37 °C in CO_2 for 15 min), dispensed in a 10 cm cell culture dish (Corning tissue culture-treated culture dishes), and incubated in at 37 °C and 5% CO_2 atmosphere (passage 1). The culture is observed under microscope twice daily.

80% confluent adherent cells are detached from the cell culture dish using trypsin/EDTA solution (3 mL of 0.25% Trypsin-0.53 mM EDTA) for 10 min and transferred into a centrifuge tube. Cells are then pelleted by centrifuging (1000g for 5 min) and resuspended in complete growth medium (3 mL). This is repeated thrice to remove trypsin. Finally, cell pellet is resuspended into 1 mL of complete growth medium, and viable cell density is measured in a Countess II cell counter (Invitrogen, MA, USA) with trypan blue (0.4% stock) 1:1 ratio.

A subculture is prepared following the same procedure as described for passage 1, and the remaining cell suspension is cryopreserved in 10% DMSO solution for future use.

Study of HEK293T Cell Transduction by rAAV Present in Crystals. In each well of a Corning Costar TC-treated 6-well plate, 2 mL of cell suspension for the passage 1 is transferred. One well serves as a negative control. Cell suspensions in two wells are transduced with standard AAV sample (Virovek) in the MOI (multiplicity of infection; number of viral genome-containing particles per cell) of 10^4, 10^5. Cell suspensions in the remaining three wells are transduced with the AAV stock solution (see the stock solution preparation section) in the MOIs and 10^4, 10^5, 10^6. Cells are then cultured in an incubator at 37 °C in 5% CO_2 atmosphere and observed in a fluorescence microscope once daily for 5 days. On day 5, cells are detached from the culture dish using trypsin/EDTA solution (3 mL of 0.25% Trypsin-0.53 mM EDTA), and viable cell density and percentage of GFP-positive cells are measured in a Countess II Cell Counter with Trypan blue (1:1; v:v, ratio of 0.4% stock). Transduction efficiency, as a percentage, is calculated by dividing GFP-positive cells by the total cell number × 100%.

TCID50 Experiment. Transduction experiments, analogous to tissue culture infectious dose (TCID50) virus assays are performed to obtain a more precise value of biologically active vector titer. In this experiment, ∼5000 cells (HEK293T cells from passage 1 as described in adherent cell culture preparation section) are seeded in each well of a 96-well plate (Corning Costar TC treated) and cultured in complete growth medium (100 μL 10%FBS in DMEM) for 2 days in a humidified incubator at 37 °C and 5% CO_2. On day 2, a dilution series of rAAV stock solution (see stock solution preparation section) is prepared using complete growth medium in a 96-well plate (Corning Costar V shaped well) with dilutions of 10^{-3}, 10^{-4}, 10^{-5}, 10^{-6}, 10^{-7}, 10^{-8}, 10^{-9}, and 10^{-10}. 100 μL of each dilution is added to each well in a column (8 wells) except for the first two columns, which are used as a negative control. The cells are then cultured (at 37 °C and 5% CO_2), and cell growth and GFP fluorescence are examined in a microscope. On day 5, the percentage of GFP-positive wells are measured and used to calculate the "TCID50" according to the Reed-Muench algorithm.[104]

Suspension Cell Culture Preparation. Flow cytometry is performed to obtain a more accurate measurement of cell viability and percentage of GFP-positive cells (transduction efficiency) than that obtained in microscopy-based approaches. Cryopreserved HEK293 F cells (Thermo Fisher Scientific) are thawed (2 min at 37 °C water bath) and dispensed into 500 μL prewarmed (at 37 °C and 5% CO_2) FreeStyle 293 expression medium (Thermo Fisher Scientific) and cultured in 20 mL of the prewarmed medium in a 150 mL Corning Erlenmeyer cell culture flask in an incubator maintained at 37 °C, 135 rpm agitation, and humidified condition with 5% CO_2. Cell viability and cell density are measured once daily in a Countess II Automated Cell Counter (Invitrogen) using Trypan blue (0.4% stock) in 1:1 ratio as described previously. Cells are passaged when viable cell density reaches 2 to 3 million per mL.

Flow Cytometry Experiment. For flow cytometry experiments, a total of nine subcultures are prepared by adding 1.1 mL HEK293 F cells (from passage 21 with 99% viability; ∼0.25 million viable cells) in 50 mL FreeStyle 293 expression medium in each Erlenmeyer shake flask (Corning) and incubating at 37 °C with 135 rpm agitation in a humidified incubator with 5% CO_2. Out of the nine subcultures, one shake flask serves as a negative control, and four shake flasks serve as a positive control, where cells are transduced with standard AAV sample (Virovek) at the following ratios of virus particles to cells or MOIs (multiplicity of infection): 10^6, 5×10^5, 10^5, and 10^4. In the remaining four shake flasks, cells are transduced with the AAV stock solution (see the stock solution preparation section)) at the same MOIs as in the positive control. Cells are incubated in an orbital shaker (at 37 °C, 5% CO_2, and 135 rpm), and aliquots are collected at 24 h intervals for flow cytometry experiments. Aggregates and cell debris are removed from the samples (0.5 mL for each experiment) by filtering in nylon

https://doi.org/10.1021/acsnano.5c00566
ACS Nano 2025, 19, 35348−35369

mesh cell strainers in polystyrene tube (Thermo Fisher Scientific). The cell viability and % GFP-positive cell numbers are measured in Aria 4 (Flow core, Koch Institute, MIT) using PI (propidium iodide) as a viability dye.

Seeding Experiments. Nucleation (primary nucleation) followed by growth of crystals in hanging drop vapor diffusion experiments (in a 24-well plate) takes about 2−3 weeks to complete, of which approximately 90% of the time belong to the induction period (i.e., time spent by the system to see the first nuclei)[105] and the remaining 2−3 days belongs to the period of visible/significant growth. For the crystallization method to be useful as an alternative purification method, the process needs to be completed within a time comparable to that of existing technologies. To evaluate the feasibility of crystallization as an alternative method for AAV purification, a crystal seed growth experiment is performed. The seed crystals themselves serve as nuclei or provide the sites for possible nucleation accelerating the nucleation process. Thus, the use of crystal seeds in a crystallization medium eliminates the nucleation step (primary nucleation) and thereby reduces the overall time for crystallization.[106] In a seeding experiment, purified/precleaned crystal seeds are added into the crystallization medium at a certain time.[107] To mimic the seeding experiment, a droplet containing well-grown crystals was identified, and growth solution (2 μL of 1:1 ratio of reservoir solution and AAV sample) was added. The variation in size of crystals is measured at 5 min to 1 h intervals in a microscope (Leica Z16 APO), and the time required for the crystals to grow to a size (minimum 10−100 μm) for it to be separable in industrial filters was measured.

Note: Primary nucleation is the initial formation of nuclei from a clear and supersaturated solution in absence of pre-existing crystals of the same compound.

Seed crystals are the already grown pieces of small crystals of the same compound and added into a crystallization system/process to promote their growth into larger crystals in a controlled manner and in a short period of time by eliminating the need of formation of uncertain/random and slow primary nuclei. Seed crystals themselves act as nuclei as well as promote the formation of smaller crystals due to many mechanisms such as collision among themselves or with the stirrer and reactor wall. These small crystals are known as secondary nuclei. These secondary nuclei grow to form larger crystals.

Yield Calculation. For the calculation of yield, droplets containing only a few distinct large crystals with no precipitate are selected, and a small volume (5 μL) of reservoir solution is mixed thoroughly with the original droplet solution. Then, 1 μL of the solution is collected using micropipette and transferred into an Amicon centrifugal filter (10 kDa NMWCO) and centrifuged at 10000g for 5 min. Capsids are then washed 3 times using 100 μL of nuclease-free water at 10000g for 5 min each time to ensure complete removal of remaining salt and precipitant. The capsid particles are then resuspended into 1 mL of Dulbecco's 1X PBS (DPBS without magnesium and calcium) and collected into a vial and stored at 4 °C for short-term use. The ELISA and the ddPCR experiments are performed to determine the quantities of total capsids and full capsids as mentioned previously. Subtracting full capsids from total capsids determines the empty capsid titer. The yield is the difference between the final and initial quantity of capsids in the solution phase divided by the initial quantity of capsids.

Scale-Up Experiment. To understand whether the preferential crystallization is relatively scalable, a microliter-volume droplet-based system was scaled up to a milliliter-volume crystallization device (Crystalline, Technobis, NL), which is widely used in the crystallization of small-molecule pharmaceuticals (please visit the reference for more detail).[108] Like the hanging drop system, the scale-up crystallizer also has an evaporation capability but, due to the flow of inert gas through the crystallization chamber, evaporation is faster in the latter. Unlike the hanging droplet system, the scaled-up reactor has a cooling jacket and a built-in stirrer. For this experiment, crystallization solution (5 mL 1:1 mixture of the rAAV sample and precipitant solution) is incubated at 30 °C for 3 h and cooled down to 18 °C and maintained there for 5 h. Solution is simultaneously evaporated by passing N_2 gas through the chamber. A small volume (100 μL) of the solution is collected into a centrifugal filter (0.1 μm pore size; Millipore Sigma) and centrifuged (1x 200g for 1 min) at room temperature. The crystals are washed with 1:1 mixture of reservoir solution and 1X PBS (2x 100 μL) at 200g followed by diH_2O (1x 100 μL; ≥18 mΩ, Milli-Q) at 2000g for 1 min. The AAV crystals are then dissolved in 300 μL of nuclease-free water at 4 °C refrigerator for 30 min, transferred into an Amicon centrifugal filter (10 kDa NMWCO), and centrifuged (10000g for 5 min). Capsids are then washed with nuclease-free water (3x 200 μL at 10000g for 5 min) and resuspended into 200 μL of Dulbecco's 1X PBS (DPBS without magnesium and calcium), and stored at 4 °C for short-term use. ddPCR and ELISA experiments are performed to determine the fraction of full and empty capsids in the crystal.

Capsid Surface Potential Measurement. *Zeta Potential Experiment.* A series of solutions of different pH (as shown in Supplementary Figure 2) for ionic strengths 0.15 and 0.2 M NaCl each is prepared using diH_2O (≥18 mΩ, Milli-Q). For each of these series solutions, 100 μL rAAV sample from the Virovek is centrifuged at 14000g for 5 min in an ultrafiltration tube to remove the PBS buffer and washed with diH_2O (≥18 mΩ, Milli-Q; 2x 100 μL at 14000g for 2 min) and resuspended in each of the series solution. The resuspended rAAV solution is loaded in a zeta potential measurement cell and the zeta potential is measured in DynaPro ZetaStar (Department of Chemistry, MIT) following the procedure as described by Wyatt Technology (MA). Measured zeta potential is plotted against the pH for each ionic strength to obtain the isoelectric point.

ASSOCIATED CONTENT

Supporting Information

The Supporting Information is available free of charge at https://pubs.acs.org/doi/10.1021/acsnano.5c00566.

Solution behavior of capsids, zeta potential measurement results, phase diagram construction from the screening of experimental conditions in a 24-well plate, individual phase diagrams for different pH values for capsids, mass spectrometry results showing post-translational modifications in Sf9 and HEK293 produced capsids, preferential crystallization regions for full and empty capsids at different pH values, preferential crystallization regions for Sf9 and HEK293 cell produced capsids, comparison of solubility and concentration explored in crystallization condition screening, crystal behavior under cross-polarized light, ddPCR and ELISA results for full and empty capsid enrichment and selectivity at different pH and precipitant concentrations, enrichment of capsids carrying transgene of lengths 1.2 kbp, 2.46 kbp, 4.68 kbp, TEM images of capsids postcrystallization, mass photometry results showing removal of partially filled capsids postpreferential crystallization, cell viability for transduction of HEK293 F cell suspension with Sf9 produced capsid serotypes 5, 8, and 9, fluorescence images of gfp positive HEK293 T cells for transduction with capsid serotypes 5, 8, and 9, sample example of $TCID_{50}$ experiment, SDS-PAGE gel electrophoretic resolution of capsid proteins with silver staining, Western blot result, EDAX analysis of capsid crystals, yield of preferential crystallization experiment at different pH and precipitant concentrations, variation of crystallization conditions as a function of AAV concentrations and precipitant concentrations (PDF)

https://doi.org/10.1021/acsnano.5c00566
ACS Nano 2025, 19, 35348−35369

AUTHOR INFORMATION

Corresponding Author

Richard D. Braatz − *Department of Chemical Engineering and Center for Biomedical Innovation, Massachusetts Institute of Technology, Cambridge, Massachusetts 02139, United States;* orcid.org/0000-0003-4304-3484; Email: braatz@mit.edu

Authors

Vivekananda Bal − *Department of Chemical Engineering, Massachusetts Institute of Technology, Cambridge, Massachusetts 02139, United States;* orcid.org/0000-0002-8204-3308

Jacqueline M. Wolfrum − *Center for Biomedical Innovation, Massachusetts Institute of Technology, Cambridge, Massachusetts 02139, United States*

Paul W. Barone − *Center for Biomedical Innovation, Massachusetts Institute of Technology, Cambridge, Massachusetts 02139, United States;* orcid.org/0000-0001-6802-6846

Stacy L. Springs − *Center for Biomedical Innovation, Massachusetts Institute of Technology, Cambridge, Massachusetts 02139, United States;* orcid.org/0000-0003-2133-5689

Anthony J. Sinskey − *Center for Biomedical Innovation and Department of Biology, Massachusetts Institute of Technology, Cambridge, Massachusetts 02139, United States;* orcid.org/0000-0002-1015-1270

Robert M. Kotin − *Center for Biomedical Innovation, Massachusetts Institute of Technology, Cambridge, Massachusetts 02139, United States; Department of Genetic & Cellular Medicine, University of Massachusetts Chan Medical School, Worcester, Massachusetts 01605, United States*

Complete contact information is available at: https://pubs.acs.org/10.1021/acsnano.5c00566

Author Contributions

V.B. conceptualized this work, designed and conducted the experiments, analyzed the data, and wrote the initial draft. P.W.B. and R.D.B. conceptualized the work, supervised the project, edited the manuscript, and acquired funds to support the project. S.L.S. contributed to supervision of the project, acquiring funds to support the project, and edited the manuscript. A.J.S. contributed to supervision of the work and acquiring the funds to support the project. R.M.K. helped in designing the experiment on the effect of transgene length, editing the manuscript, and acquiring the funds to support the project. J.M.W. contributed to supervising the work, editing the manuscript, and acquired the funds to support the project.

Notes

The authors declare the following competing financial interest(s): The authors have filed a patent (US Patent App. 18/732,263) related to this work.

ACKNOWLEDGMENTS

Funding is acknowledged from the MLSC, Sanofi, Sartorius, Artemis, and US FDA (75F40121C00131). Andreas Lucas Gimpel is acknowledged for training the first author in the earlier crystallization experimental work. Moo Sun Hong is acknowledged for preliminary training in use of the polarizer instrument. Jose Sangerman is acknowledged for training in the first experiment of suspension cell culture preparation. John Joseph and Jose Sangerman are acknowledged for training in the first ddPCR and ELISA experiments. Help of Prasanna Srinivasan in the first adherent cell culture preparation is acknowledged. Help of Rui Wen Ou in the first electrophoresis experiment is acknowledged. Operators Young Zhang and Zhen-yuan Zhang at MIT.Nano, Dong Soo Yun and Daniel Cham Chin Lim at the Koch Institute, and Kayleigh Fay at Refeyn (Waltham, MA) are acknowledged for discussion of crystallography and material characterization methods.

REFERENCES

(1) Valdmanis, P. N.; Kay, M. A. Future of rAAV gene therapy: Platform for RNAi, gene editing, and beyond. *Hum. Gene Ther.* **2017**, *28*, 361−372.

(2) Ma, C. C.; Wang, Z. L.; Xu, T.; He, Z. Y.; Wei, Y. Q. The approved gene therapy drugs worldwide: from 1998 to 2019. *Biotechnol Adv.* **2020**, *40*, 107502.

(3) Ginn, S. L.; Amaya, A. K.; Alexander, I. E.; Edelstein, M.; Abedi, M. R. Gene therapy clinical trials worldwide to 2017: An update. *Journal of Gene Medicine* **2018**, *20*, e3015.

(4) Dunbar, C. E.; et al. Gene therapy comes of age. *Science (1979)* **2018**, *359*, eaan4672.

(5) Zeltner, N.; Kohlbrenner, E.; Clément, N.; Weber, T.; Linden, R. M. Near-perfect infectivity of wild-type AAV as benchmark for infectivity of recombinant AAV vectors. *Gene Ther.* **2010**, *17*, 872−879.

(6) Sommer, J. M.; et al. Quantification of adeno-associated virus particles and empty capsids by optical density measurement. *Molecular Therapy* **2003**, *7*, 122−128.

(7) Schnödt, M.; Büning, H. Improving the quality of adeno-associated viral vector preparations: The challenge of product-related impurities. *Hum Gene Ther Methods* **2017**, *28*, 101−108.

(8) Gao, K.; et al. Empty virions in AAV8 vector preparations reduce transduction efficiency and may cause total viral particle dose-limiting side effects. *Mol. Ther Methods Clin Dev* **2014**, *1*, 9.

(9) Timmers, A. M.; et al. Ocular inflammatory response to intravitreal injection of adeno-associated virus vector: Relative contribution of genome and capsid. *Hum. Gene Ther.* **2020**, *31*, 80−89.

(10) Guillou, J.; et al. Fatal thrombotic microangiopathy case following adeno-associated viral SMN gene therapy. *Blood Adv.* **2022**, *6*, 4266−4270.

(11) Venkatakrishnan, B.; et al. Structure and dynamics of adeno-associated virus serotype 1 VP1-unique N-terminal domain and its role in capsid trafficking. *J. Virol Methods* **2013**, *87*, 4974−4984.

(12) Senapathy, P.; Carter, B. J. Molecular cloning of adeno-associated virus variant genomes and generation of infectious virus by recombination in mammalian cells. *J. Biol. Chem.* **1984**, *259*, 4661−4666.

(13) Khatwani, S. L.; Pavlova, A.; Pirot, Z. Anion-exchange HPLC assay for separation and quantification of empty and full capsids in multiple adeno-associated virus serotypes. *Mol. Ther Methods Clin Dev* **2021**, *21*, 548−558.

(14) Nass, S. A.; et al. Universal method for the purification of recombinant AAV vectors of differing serotypes. *Mol. Ther Methods Clin Dev* **2018**, *9*, 33−46.

(15) Chen, H.; Marino, S.; Ho, C. Y. Large scale purification of AAV with continuous flow ultracentrifugation. *Molecular Therapy* **2016**, *24*, S42.

(16) Yu, Z.; et al. TPP combined with DGUC as an economic and universal process for large-scale purification of AAV vectors. *Mol. Ther Methods Clin Dev* **2020**, *17*, 34−48.

(17) Qu, W.; Wang, M.; Wu, Y.; Xu, R. Scalable downstream strategies for purification of recombinant adeno- associated virus vectors in light of the properties. *Curr. Pharm. Biotechnol* **2015**, *16*, 684−695.

(18) Everts, J. C.; Ravnik, M. Complex electric double layers in charged topological colloids. *Sci. Rep* **2018**, *8*, 14119.
(19) Salis, A.; et al. Measurements and theoretical interpretation of points of zero charge/potential of BSA protein. *Langmuir* **2011**, *27*, 11597−11604.
(20) Wennerström, H.; Estrada, E. V.; Danielsson, J.; Oliveberg, M. Colloidal stability of the living cell. *Proc. Natl. Acad. Sci. U.S.A.* **2020**, *117*, 10113−10121.
(21) Salgın, S.; Salgın, U.; Bahadır, S. Zeta potentials and isoelectric points of biomolecules: the effects of ion types and ionic strengths. *Int. J. Electrochem. Sci.* **2012**, *7*, 12404−12414.
(22) Dukhin, A. S.; Parlia, S. Measuring zeta potential of protein nano-particles using electroacoustics. *Colloids Surf. B Biointerfaces* **2014**, *121*, 257−263.
(23) Yamanaka, M.; et al. Optimization of salt concentration in PEG-based crystallization solutions. *J. Synchrotron Radiat* **2011**, *18*, 84−87.
(24) Warren, P. B. Simple models for charge and salt effects in protein crystallisation. *J. Phys. Cond. Mater.* **2002**, *14*, 7617.
(25) Schmit, J. D.; Dill, K. Growth rates of protein crystals. *J. Am. Chem. Soc.* **2012**, *134*, 3934−3937.
(26) Li, X.; et al. Charged polymeric additives affect the nucleation of lysozyme crystals. *CrystEngComm* **2019**, *21*, 1992−2001.
(27) Kung, W.; Gonzalez-Mozuelos, P.; de la Cruz, M. O. Nanoparticles in aqueous media: crystallization and solvation charge asymmetry. *Soft Matter* **2010**, *6*, 331−341.
(28) Ioka, M.; et al. Crystallization of charged gold particles mediated by nonadsorbing like-charged polyelectrolyte. *J. Chem. Phys.* **2021**, *154*, 234901.
(29) Bishop, K. J. M.; Chevalier, N. R.; Grzybowski, B. A. When and why like-sized, oppositely charged particles assemble into diamond-like crystals. *J. Phys. Chem. Lett.* **2013**, *4*, 1507−1511.
(30) Mary, B.; Maurya, S.; Arumugam, S.; Kumar, V.; Jayandharan, G. R. Post-translational modifications in capsid proteins of recombinant adeno-associated virus (AAV) 1-rh10 serotypes. *FEBS J.* **2019**, *286*, 4964−4981.
(31) Fang, N. X.; Frazer, I. H.; Fernando, G. J. Differences in the post-translational modifications of human papillomavirus type 6b major capsid protein expressed from a baculovirus system compared with a vaccinia virus system. *Biotechnol Appl. Biochem* **2000**, *32*, 27−33.
(32) Bonneté, F. Colloidal approach analysis of the marseille protein crystallization database for protein crystallization strategies. *Cryst. Growth Des* **2007**, *7*, 2176−2181.
(33) Charles, M.; Veesler, S.; Bonneté, F. MPCD: A new interactive on-line crystallization data bank for screening strategies. *Acta Crystallogr. D Biol. Crystallogr.* **2006**, *62*, 1311−1318.
(34) Weber, M.; Jones, M. J.; Ulrich, J. Crystallization as a purification method for jack bean urease: On the suitability of poly(ethylene glycol), Li 2so 4, and NaCl as precipitants. *Cryst. Growth Des* **2008**, *8*, 711−716.
(35) McPherson, A.; Gavira, J. A. Introduction to protein crystallization. *Acta Crystallogr. F Struct Biol. Commun.* **2014**, *70*, 2−20.
(36) Tang, S. K.; Davey, R. J.; Sacchi, P.; Cruz-Cabeza, A. J. Can. molecular flexibility control crystallization? The case of para substituted benzoic acids. *Chem. Sci.* **2021**, *12*, 993−1000.
(37) Yu, L.; Reutzel-Edens, S. M.; Mitchell, C. A. Crystallization and polymorphism of conformationally flexible molecules: problems, patterns, and strategies. *Org. Process Res. Dev* **2000**, *4*, 396−402.
(38) Wicker, J. G. P.; Cooper, R. I. Will it crystallise? Predicting crystallinity of molecular materials. *CrystEngComm* **2015**, *17*, 1927−1934.
(39) Shaw, K. L.; Grimsley, G. R.; Yakovlev, G. I.; Makarov, A. A.; Pace, C. N. The effect of net charge on the solubility, activity, and stability of ribonuclease Sa. *Protein science* **2001**, *10*, 1206−1215.
(40) Alberts, B. et al.. *Molecular Biology of the Cell*, 4th ed.; Garland Science: New York, 2002.
(41) Nadendla, K.; Friedman, S. H. Light control of protein solubility through isoelectric point modulation. *J. Am. Chem. Soc.* **2017**, *139*, 17861−17869.
(42) Sun, X.; et al. Role of protein charge density on hepatitis B virus capsid formation. *ACS Omega* **2018**, *3*, 4384−4391.
(43) McGarvey, P. W.; Hoffmann, M. M. Solubility of some mineral salts in polyethylene glycol and related surfactants. *Tenside, Surfactants, Detergents* **2018**, *55*, 203−209.
(44) Soleymani, J.; Jouyban-Gharamaleki, V.; Kenndler, E.; Jouyban, A. Measurement and modeling of sodium chloride solubility in binary mixtures of water + polyethylene glycol 400 at various temperatures. *J. Mol. Liq.* **2020**, *316*, 113777.
(45) Heeb, R.; Lee, S.; Venkataraman, N. V.; Spencer, N. D. Influence of salt on the aqueous lubrication properties of end-grafted, ethylene glycol-based self-assembled monolayers. *ACS Appl. Mater. Interfaces* **2009**, *1*, 1105−1112.
(46) Brunchi, C. E.; Ghimici, L. PEG in aqueous salt solutions. Viscosity and separation ability in a TiO2 suspension. *Revue Roumaine de Chimie* **2013**, *58*, 183−188.
(47) Rumachik, N. G.; et al. Methods matter: standard production platforms for recombinant AAV produce chemically and functionally distinct vectors. *Mol. Ther Methods Clin Dev* **2020**, *18*, 98−118.
(48) Liu, S.; et al. Systematic comparison of rAAV vectors manufactured using large-scale suspension cultures of Sf9 and HEK293 cells. *Molecular Therapy* **2024**, *32*, 74−83.
(49) Back, K. R.; Davey, R. J.; Grecu, T.; Hunter, C. A.; Taylor, L. S. Molecular conformation and crystallization: The case of Ethenzamide. *Cryst. Growth Des* **2012**, *12*, 6110−6117.
(50) Chen, R. Q.; et al. An investigation of the effects of varying pH on protein crystallization screening. *Crystal Engineering Communication* **2017**, *19*, 860−867.
(51) McColl-Carboni, A.; et al. Analytical characterization of full, intermediate, and empty AAV capsids. *Gene Ther.* **2024**, *31*, 285−294.
(52) Kurth, S.; et al. Separation of full and empty adeno-associated virus capsids by anion-exchange chromatography using choline-type salts. *Anal. Biochem.* **2024**, *686*, 115421.
(53) Wright, J. F. Product-related impurities in clinical-grade recombinant AAV vectors: characterization and risk assessment. *Biomedicines* **2014**, *2*, 80−97.
(54) Rieser, R.; et al. Comparison of different liquid chromatography-based purification strategies for adeno-associated virus vectors. *Pharmaceutics* **2021**, *13*, 748.
(55) Cerritelli, M. E.; et al. Encapsidated conformation of Bacteriophage T7 DNA. *Cell* **1997**, *91*, 271−280.
(56) Perini, G. *Predictive design of filtration processes in the pharmaceutical industry - the impact of crystal size and shape*, Ph.D. Thesis. The University of Manchester, Manchester, 2020.
(57) Marichal-Gallardo, P.; et al. Single-use capture purification of adeno-associated viral gene transfer vectors by membrane-based steric exclusion chromatography. *HUM GENE THER.* **2021**, *32*, 959−974.
(58) Tomono, T.; et al. Ultracentrifugation-free chromatography-mediated large-scale purification of recombinant adeno-associated virus serotype 1 (rAAV1). *Mol. Ther Methods Clin Dev* **2016**, *3*, 15058.
(59) Tomono, T.; et al. Highly efficient ultracentrifugation-free chromatographic purification of recombinant AAV serotype 9. *Mol. Ther Methods Clin Dev* **2018**, *11*, 180−190.
(60) Okada, T.; et al. Scalable purification of adeno-associated virus serotype 1 (AAV1) and AAV8 vectors, using dual ion-exchange adsorptive membranes. *Hum. Gene Ther.* **2009**, *20*, 1013−1021.
(61) Jungmann, A.; Leuchs, B.; Rommelaere, J.; Katus, H. A.; Müller, O. J. Protocol for efficient generation and characterization of adeno-associated viral vectors. *Hum Gene Ther Methods* **2017**, *28*, 235−246.
(62) Strobel, B.; Miller, F. D.; Rist, W.; Lamla, T. Comparative analysis of cesium chloride- and iodixanol-based purification of recombinant adeno-associated viral vectors for preclinical applications. *Hum Gene Ther Methods* **2015**, *26*, 147−157.

https://doi.org/10.1021/acsnano.5c00566
ACS Nano 2025, 19, 35348−35369

(63) Neveu, E. et al.. Case study: evaluation of several process cell lysis reagents as replacements for triton X-100 for rAAV production. https://www.skpharmteco.com/news-insights/case-study/case-study-evaluation-of-several-process-cell-lysis-reagents-as-replacements-for-triton-x-100-for-raav-production/ (2025).
(64) Prebeg, T.; Omerčić, D.; Erceg, V.; Matijašić, G. Comparison of sodium lauryl sulfate and sodium lauryl ether sulfate detergents for decellularization of porcine liver for tissue engineering applications. *Chem. Eng. Trans* **2023**, *100*, 745−750.
(65) Yang, C.; Mao, Z. *Numerical Simulation of Multiphase Reactors with Continuous Liquid Phase*; Elsevier Ltd, 2014.
(66) MSMPR Crystallizer. https://www.mt.com/gb/en/home/applications/L1_AutoChem_Applications/L2_Crystallization/msmpr-crystallizer.html#overviewaf (2025).
(67) Qu, G.; et al. Separation of adeno-associated virus type 2 empty particles from genome containing vectors by anion-exchange column chromatography. *J. Virol Methods* **2007**, *140*, 183−192.
(68) Effective separation of full and empty adeno-associated virus capsids by anion exchange. https://www.cytivalifesciences.com/en/us/solutions/cell-therapy/knowledge-center/resources/effective-separation-of-full-and-empty-raav-capsids-by-anion-exchange?srsltid=AfmBOop-WhScvLN7x9vGL_PnmmBMkcW0hdfonVj8dutA__aEogWukN3Z (2024).
(69) Dickerson, R.; Argento, C.; Pieracci, J.; Bakhshayeshi, M. Separating empty and full recombinant adeno-associated virus particles using isocratic anion exchange chromatography. *BioTechnology J.* **2021**, *16*, 2000015.
(70) Croyle, M.; Cheng, X.; Wilson, J. M. Development of formulations that enhance physical stability of viral vectors for gene therapy. *Gene Ther.* **2001**, *8*, 1281−1290.
(71) Gruntman, A. M.; et al. Stability and compatibility of recombinant adeno-associated virus under conditions commonly encountered in human gene therapy trials. *Hum Gene Ther Methods* **2015**, *26*, 71−76.
(72) Xie, Q.; Hare, J.; Turnigan, J.; Chapman, M. S. Large-scale production, purification and crystallization of wild-type adeno-associated virus-2. *J. Virol Methods* **2004**, *122*, 17−27.
(73) Kaludov, N. E. P.; et al. Production, purification and preliminary X-ray crystallographic studies of adeno-associated virus serotype 4. *Virology* **2003**, *306*, 1−6.
(74) Lins-Austin, B.; et al. Adeno-associated virus (AAV) capsid stability and liposome remodeling during endo/lysosomal pH trafficking. *Viruses* **2020**, *12*, 668.
(75) Stevenson, H. P.; et al. Transmission electron microscopy for the evaluation and optimization of crystal growth. *Acta Crystallogr. D Struct Biol.* **2016**, *72*, 603−615.
(76) Xie, Q.; et al. The atomic structure of adeno-associated virus (AAV-2), a vector for human gene therapy. *Proc. Natl. Acad. Sci. U. S. A.* **2002**, *99*, 10405−10410.
(77) Xie, Q.; Ongley, H. M.; Hare, J.; Chapman, M. S. Crystallization and preliminary X-ray structural studies of adeno-associated virus serotype 6. *Acta Crystallogr. Sect F Struct Biol. Cryst. Commun.* **2008**, *64*, 1074−1078.
(78) Mitchell, M.; et al. Production, purification and preliminary X-ray crystallographic studies of adeno-associated virus serotype 9. *Acta Crystallogr. Sect F Struct Biol. cryst Commun.* **2009**, *65*, 715−718.
(79) Singer, W.; Rubinsztein-Dunlop, H.; Gibson, U. Manipulation and growth of birefringent protein crystals in optical tweezers. *Opt Express* **2004**, *12*, 6440−6445.
(80) Echalier, A.; Glazer, R. L.; Fülöp, V.; Geday, M. A. Assessing crystallization droplets using birefringence. *Acta Crystallogr. D structural biology* **2004**, *60*, 696−702.
(81) Murphy, D. B., Spring, K. R., Fellers, T. J.; Davidson, M. W. Principles of Birefringence. https://www.microscopyu.com/techniques/polarized-light/principles-of-birefringence (2025).
(82) Bloss, F. D. *Crystallography and Crystal Chemistry*; Hold, Rinehart, Winston, Inc.: New York, NY, 1971.
(83) Dyar, M. D.; Gunter, M. E.; Tasa, D. *Mineralogy and Optical Mineralogy*, 2nd ed.; Mineralogical Society of America: Chantilly, VA, 2020.
(84) Nesse, W. D. *Introduction to Optical Mineralogy*, 3rd ed.; Oxford University Press, 2003.
(85) Polowsky, P. J.; Tansman, G. F.; Kindstedt, P. S.; Hughes, J. M. Characterization and identification of surface crystals on smear-ripened cheese by polarized light microscopy. *J. Dairy Sci.* **2018**, *101*, 7714−7723.
(86) Rieser, R.; Menzen, T.; Biel, M.; Michalakis, S.; Winter, G. Systematic studies on stabilization of AAV vector formulations by lyophilization. *J. Pharm. Sci.* **2022**, *111*, 2288−2298.
(87) AAV9 Xpress ELISA kit. https://us.progen.com/AAV9-Xpress-ELISA/PRAAV9XP?etcc_med=SEA&etcc_par=Google&etcc_cmp=20979150126&etcc_grp=166934735908&etcc_bky=progen%20aav9%20elisa&etcc_mty=p&etcc_plc=&etcc_ctv=689492155813&etcc_bde=c&etcc_var=Cj0KCQjwqIm_BhDnARIsAKBYcmskle2tb-0SuGxZr5pRF3KaH0ElvEiZamWQmaAEzjHPVnP_S0M2MS8aAv6_EALw_wcB&gad_source=1&gclid=Cj0KCQjwqIm_BhDnARIsAKBYcmskle2tb-0SuGxZr5pRF3KaH0ElvEiZamWQmaAEzjHPVnP_S0M2MS8aAv6_EALw_wcB (2025).
(88) AAV8 Xpress ELISA kit. https://us.progen.com/AAV8-Xpress-ELISA/PRAAV8XP (2025).
(89) AAV5 Xpress ELISA kit. https://us.progen.com/AAV5-Xpress-ELISA/PRAAV5XP (2025).
(90) Nguyen, T. N. T.; et al. Mechanistic model for production of recombinant adeno-associated virus via triple transfection of HEK293 cells. *Molecular Therapy - Methods & Clinical Development* **2021**, *21*, 642−655.
(91) Droplet Digital PCR applicaitons guide. https://www.bio-rad.com/webroot/web/pdf/lsr/literature/Bulletin_6407.pdf (2024).
(92) Nguyen, H. T.; et al. Single-capsid identification of full and empty status of recombinant adeno-associated viruses via resistive pulse sensing. *Sensors and Actuators Reports* **2024**, *8*, 100242.
(93) Wu, D.; Piszczek, G. Standard protocol for mass photometry experiments. *Eur. Biophys J.* **2021**, *50*, 403−409.
(94) S-Trap™ micro spin column digestion protocol. https://files.protifi.com/protocols/s-trap-micro-long-4-7.pdf (2024).
(95) Oyama, H.; Ishii, K.; Maruno, T.; Torisu, T.; Uchiyama, S. Characterization of adeno-associated virus capsid proteins with two types of VP3-related components by capillary gel electrophoresis and mass spectrometry. *Hum. Gene Ther.* **2021**, *32*, 1403−1416.
(96) Mini-PROTEAN Tetra Vertical Electrophoresis Cell. https://www.bio-rad.com/en-us/product/mini-protean-tetra-vertical-electrophoresis-cell?ID=N3F2UD4VY (2024).
(97) Zhou, Y.; et al. Adeno-associated virus serotype 2 capsids with proteolytic cuts by trypsin remain intact and potent. *Gene Ther.* **2025**, *32*, 121−131.
(98) Silver stain plus kit. https://www.bio-rad.com/en-us/product/silver-stain-plus-kit?ID=02933b12-38b0-46d4-a9af-f0e96973c029 (2024).
(99) SimplyBlue Safe Stain Protocol. https://www.thermofisher.com/us/en/home/references/protocols/proteins-expression-isolation-and-analysis/staining-protein-gels/coomassie-staining.html (2024).
(100) Western blot protocol. https://www.abcam.com/en-us/technical-resources/protocols/western-blot?srsltid=AfmBOooekOsNgXBKNiqZSKGE0c0cnjhyT_NXwIVio8sgnjvNDHzZZK8i (2022).
(101) EDAX Trident (EDS-EBSD-WDS) System. https://www.edax.com/products/integrated-technologies/trident (2023).
(102) Ares, J. R.; Pascual, A.; Ferrer, I. J.; Sanchez, C. A methodology to reduce error sources in the determination of thin film chemical composition by EDAX. *Thin Solid Films* **2004**, *450*, 207−210.
(103) Smith, D. J.; McCartney, M. R. Microscopy applications: Semiconductors. *Encyclopedia of Analytical Science* **2005**, 84−91.

https://doi.org/10.1021/acsnano.5c00566
ACS Nano 2025, 19, 35348−35369

(104) Lei, C.; Yang, J.; Hu, J.; Sun, X. On the calculation of TCID50 for quantitation of virus infectivity. *Virologica Sinica* **2021**, *36*, 141−144.
(105) Chen, K.; et al. Identification of nucleation rates in droplet-based microfluidic systems. *Chem. Eng. Sci.* **2012**, *77*, 235−241.
(106) Developing seeding protocols through secondary nucleation measurements on the Crystalline. https://www.crystallizationsystems.com/news/developing-seeding-protocols-through-secondary-nucleation-measurements-on-the-crystalline/ (2023).
(107) Briuglia, M.; Sefcik, J.; ter Horst, J. Measuring secondary nucleation through single crystal seeding. *Cryst. Growth Des.* **2019**, *19*, 421−429.
(108) Crystalline. Every picture tells your story. https://www.crystallizationsystems.com/products/crystalline/ (2024).

https://doi.org/10.1021/acsnano.5c00566
ACS Nano 2025, 19, 35348−35369